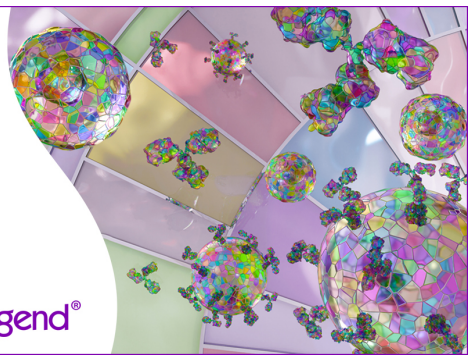

The Journal of Immunology
RESEARCH ARTICLE | JULY 15 2015

Inhibition of System $_{Xc}^-$ Transporter Attenuates Autoimmune Inflammatory Demyelination FREE

Kirsten S. Evonuk; ... et. al

J Immunol (2015) 195 (2): 450–463.
https://doi.org/10.4049/jimmunol.1401108

Inhibition of System $_{Xc}^-$ Transporter Attenuates Autoimmune Inflammatory Demyelination

Kirsten S. Evonuk,[*,†,1] Brandi J. Baker,[*,†,1] Ryan E. Doyle,[*,†] Carson E. Moseley,[‡] Christine M. Sestero,[§,¶] Bryce P. Johnston,[*,†] Patrizia De Sarno,[‖] Andrew Tang,[†] Igor Gembitsky,[†] Sandra J. Hewett,[#] Casey T. Weaver,[‡] Chander Raman,[§] and Tara M. DeSilva[*,†,]**

T cell infiltration into the CNS is a significant underlying pathogenesis in autoimmune inflammatory demyelinating diseases. Several lines of evidence suggest that glutamate dysregulation in the CNS is an important consequence of immune cell infiltration in neuroinflammatory demyelinating diseases; yet, the causal link between inflammation and glutamate dysregulation is not well understood. A major source of glutamate release during oxidative stress is the system $_{Xc}^-$ transporter; however, this mechanism has not been tested in animal models of autoimmune inflammatory demyelination. We find that pharmacological and genetic inhibition of system $_{Xc}^-$ attenuates chronic and relapsing-remitting experimental autoimmune encephalomyelitis (EAE). Remarkably, pharmacological blockade of system $_{Xc}^-$ 7 d after induction of EAE attenuated T cell infiltration into the CNS, but not T cell activation in the periphery. Mice harboring a Slc7a11 (xCT) mutation that inactivated system $_{Xc}^-$ were resistant to EAE, corroborating a central role for system $_{Xc}^-$ in mediating immune cell infiltration. We next examined the role of the system $_{Xc}^-$ transporter in the CNS after immune cell infiltration. Pharmacological inhibitors of the system $_{Xc}^-$ transporter administered during the first relapse in a SJL animal model of relapsing-remitting EAE abrogated clinical disease, inflammation, and myelin loss. Primary coculture studies demonstrate that myelin-specific CD4$^+$ Th1 cells provoke microglia to release glutamate via the system $_{Xc}^-$ transporter, causing excitotoxic death to mature myelin-producing oligodendrocytes. Taken together, these studies support a novel role for the system $_{Xc}^-$ transporter in mediating T cell infiltration into the CNS as well as promoting myelin destruction after immune cell infiltration in EAE. ***The Journal of Immunology*****, 2015, 195: 450–463.**

Autoimmune inflammatory demyelinating diseases, such as multiple sclerosis (MS), are initiated by activated T cells specific for myelin Ags. Myelin-specific T cells infiltrate the CNS, triggering an inflammatory response resulting in white matter lesions marked by myelin destruction and axonal injury. Myelin plays a dual role, enhancing saltatory action potential propagation as well as protecting nerve fibers from injury (1). Recent studies suggest that myelin also provides metabolic support to axons (2). Current treatments in MS focus on attenuating immune cell infiltration into the CNS. These treatments decrease the number of relapses, but do not completely eliminate them (i.e., immune cell infiltration into the CNS), warranting treatment strategies that protect the myelin-axon unit.

Mechanisms underlying demyelination in autoimmune diseases are not well understood, although inflammation unequivocally plays an important role. One consequence of inflammation may be the accumulation of glutamate resulting in excitotoxicity. Excitotoxicity is a pathological consequence of prolonged activation of glutamate receptors resulting in excessive influx of calcium into the cytosol, leading to cell death. Excitotoxic neuronal cell death is a common pathway of injury in many neurologic diseases. Excitotoxicity has also been implicated in injury to premyelinating oligodendrocytes (OLs) in disorders of developing cerebral white matter (3–5) as well as to mature myelin in adult white matter injury (6–9). Excitotoxicity as a mechanism in autoimmune encephalomyelitis is supported by animal studies in which blocking the α-amino-3-hydroxy-5-methyl-4-isoxazolepropionic acid (AMPA)–type glutamate receptor prevents myelin degradation (10–13). Evidence in this regard is further substantiated by studies in MS patients in which elevated levels of glutamate are found in white matter lesions and cerebrospinal fluid (14, 15). However, the source of excitotoxic glutamate remains unclear.

Release of glutamate from the system $_{Xc}^-$ transporter is a well-known source of glutamate toxicity during oxidative stress (16, 17).

*Center for Glial Biology in Medicine, University of Alabama at Birmingham, Birmingham, AL 35294; †Department of Physical Medicine Rehabilitation, University of Alabama at Birmingham, Birmingham, AL 35294; ‡Department of Pathology, University of Alabama at Birmingham, Birmingham, AL 35294; §Department of Medicine, University of Alabama at Birmingham, Birmingham, AL 35294; ¶Department of Biology, Chemistry, and Mathematics, University of Montevallo, Montevallo, AL 35115; ‖Department of Cell, Developmental, and Integrative Biology, University of Alabama at Birmingham, Birmingham, AL 35294; #Program in Neuroscience, Department of Biology, Syracuse University, Syracuse, NY 13244; and **Department of Neurobiology, University of Alabama at Birmingham, Birmingham, AL 35294

[1]K.S.E. and B.J.B. contributed equally to this manuscript.

Received for publication May 1, 2014. Accepted for publication May 11, 2015.

This work was supported by National Institute of Neurological Disorders and Stroke Grant P30-NS069324, the National Multiple Sclerosis Society (RG 4587-A-1), the National Science Foundation (IOS-1355183), the Civitan International Research Foundation, the Mike L. Jezdimir Transverse Myelitis Foundation, the University of Alabama Health Services Foundation–General Endowment Fund, and Grant T32 AI007051 from the National Institute of Allergy and Infectious Diseases, National Institutes of Health.

Address correspondence and reprint requests to Dr. Tara M. DeSilva, 1825 University Boulevard, Shelby 503, Center for Glial Biology in Medicine, Department of Physical Medicine and Rehabilitation, University of Alabama at Birmingham, Birmingham, AL 35233. E-mail address: desilvat@uab.edu

The online version of this article contains supplemental material.

Abbreviations used in this article: AMPA, α-amino-3-hydroxy-5-methyl-4-isoxazolepropionic acid; DAB, diaminobenzidine; EAE, experimental autoimmune encephalomyelitis; EdU, 5-ethynyl-2′-deoxyuridine; GFAP, glial fibrillary acidic protein; iNOS, inducible NO synthase; MOG, myelin OL glycoprotein; MS, multiple sclerosis; NMDA, *N*-methyl-D-aspartate; OL, oligodendrocyte; PFA, paraformaldehyde; PLP, proteolipid protein; SAS, sulfasalazine; *S*-4-CPG, (*S*)-4-carboxyphenylglycine.

The system $_{Xc}^{-}$ transporter imports L-cystine into the cell to be used in the metabolism of the cellular antioxidant glutathione in exchange for the export of glutamate. This mechanism may be important for the survival of reactive glia in oxidizing environments because cultured macrophages deficient in system $_{Xc}^{-}$ die in response to inflammatory stimuli unlike wild-type macrophages (18). Futhermore, gliomas (cancerous glial cells) upregulate the system $_{Xc}^{-}$ transporter, increasing their antioxidant defense at the expense of killing neurons by excitotoxicity (19). LPS-activated microglia in vitro release glutamate through the system $_{Xc}^{-}$ transporter to induce OL excitotoxicity (20); however, this mechanism has not been tested in vivo or in models of autoimmune inflammatory demyelination.

To explore the link between inflammation and glutamate dysregulation in autoimmune inflammatory demyelination, we used pharmacological inhibition as well as genetic alteration of system $_{Xc}^{-}$. Unexpectedly, we found that genetic deletion or pharmacological inhibition of the system $_{Xc}^{-}$ transporter reduced T cell infiltration in the CNS in experimental autoimmune encephalomyelitis (EAE). No reduction in T cell proliferation was found in spleens, suggesting that altering the function of system $_{Xc}^{-}$ did not affect T cell activation, but rather perturbed infiltration into the CNS. These data support a critical role for system $_{Xc}^{-}$ in immune cell infiltration into the CNS in chronic EAE. To examine the hypothesis that cytokine-mediated excitotoxic oligodendrocyte death is initiated by myelin OL glycoprotein (MOG)–specific Th cells, pharmacological inhibition of system $_{Xc}^{-}$ was performed after immune cell infiltration in a relapsing-remitting model of EAE. Blocking system $_{Xc}^{-}$ in this regard attenuated clinical scores, which was consistent with a reduction in both reactive gliosis and myelin damage. Furthermore, we demonstrated that myelin-specific $CD4^+$ Th1 cells coopt microglia to release glutamate via the system $_{Xc}^{-}$ transporter, resulting in mature OL death. These findings suggest that system $_{Xc}^{-}$ not only promotes excitotoxic damage to myelin, ultimately linking inflammation to excitotoxicity, but also plays an important role in peripheral immune cell infiltration in autoimmune inflammatory demyelinating diseases.

Materials and Methods

Animals

Male C57BL/6 mice were purchased from Charles River Laboratories (Wilmington, MA) or The Jackson Laboratory (Bar Harbor, ME), and female SJL mice were purchased from National Cancer Institute–Frederick Cancer Research (Frederick, MD). Timed pregnant female rats were obtained from Charles River Laboratories. All animals were housed and treated in accordance with National Institutes of Health and University of Alabama at Birmingham Institutional Animal Care and Use Committee guidelines. Female wild-type C3H/HeSnJ and C3H/HeSnJ-Slc7a11$^{sut/sut}$ littermates for these studies were derived from hemizygous C3H/HeSnJ-Slc7a11$^{sut/+}$ (The Jackson Laboratory 001310) breeding units maintained at Syracuse University's laboratory animal resource facility in accordance with their institutional animal care and use guidelines. Genotyping was performed as previously described (21).

Oligodendrocyte and microglia cultures

OLs and microglia were obtained from postnatal day 2 or 3 Long–Evans rats using previously described methods (22). Mixed glia were grown on poly-D-lysine–coated flasks in DMEM (Life Technologies/Invitrogen, Carlsbad, CA) containing 20% FBS (Hyclone/Thermo Scientific, Rockford, IL) and 1.2% penicillin/streptomycin (Life Technologies/Invitrogen, Carlsbad, CA) for 10 d. Flasks were then shaken at 200 rpm, 37˚C for 1 h to isolate microglia. Following removal of microglia, OLs were obtained by shaking at 200 rpm, 37˚C for 18 h. Purified OLs were plated onto poly-DL-ornithine–coated plates and maintained in basal defined media (DMEM containing 4 mM L-glutamine, 1 mM pyruvic acid, 1 mg/ml BSA, 50 μg/ml human apo-transferrin, 5 μg/ml bovine pancreatic insulin, 30 nM sodium selenite, 10 nM D-biotin, and 10 nM hydrocortisone) supplemented with recombinant basic fibroblast growth factor (10 ng/ml; PeproTech, Rocky Hill, NJ) and human platelet-derived growth factor (10 ng/ml; PeproTech) for 7 d. To promote differentiation into mature (myelin-producing) OLs, cells were then cultured for another 7 d in basal defined media containing triiodothyronine (3 ng/ml; PeproTech) and ciliary neurotrophic factor (10 ng/ml; PeproTech). Mature OLs identified as myelin basic protein–expressing cells, as previously described (22), were used in these studies. OL cultures are typically 95% OLs, 1–2% astrocytes, and 1–2% microglia.

Immunocytochemistry of primary cultured mature OLs

Only mature OLs staining positive for myelin basic protein (1:1000; Covance, SMI-99P), as described (22), were used for studies in this manuscript. To quantify survival, immunocytochemical staining of remaining mature OLs was performed. This approach was taken as opposed to staining for cell injury markers because only surviving mature OLs remained adhered to the plate. Mature OLs were fixed in 4% paraformaldehyde (PFA), washed in PBS (in mM: 10 sodium phosphate, 2 potassium phosphate, 2.7 potassium chloride, and 137 sodium chloride [pH 7.4]) containing 0.1% Triton-X 100 (Sigma-Aldrich, St. Louis, MO), and blocked with 5% goat serum (Life Technologies/Invitrogen, Carlsbad, CA). Mature OLs were stained with anti-Olig2 mAb (1:2000; Millipore, MABN50) and detected with goat anti-mouse IgG conjugated to Alexa Fluor 488 or Alexa Fluor 594 (1:1000; Invitrogen, A-11029 and A-11032, respectively). Cells were counted on a fluorescent Nikon Eclipse Ti microscope using automated NIS-Elements software (Melville, NY).

Generation and characterization of $MOG_{35–55}$-specific Th1 and Th17 cells

$MOG_{35–55}$-specific (MOGp) Th1 and Th17 cells were generated as described previously (23, 24). Briefly, splenocytes and draining lymph node cells were obtained from male C57BL/6 mice 12 d postimmunization with 150 μg MOGp (CPC Scientific, San Jose, CA) in CFA. The mononuclear cell preparation was depleted of B cells and $CD8^+$ T cells by magnetic bead chromatography using Dynabeads Biotin Binder (Invitrogen, Grand Island, NY). The CD4-enriched mononuclear cells were differentiated to Th1 or Th17 and characterized as described previously (24). All Abs were obtained from BioLegend (San Diego, CA).

Coculture of microglia, mature OLs, and Th cells

Mature OLs were cocultured with Th1 or Th17 cells (4×10^5) in the presence or absence of microglia (1×10^5) for toxicity and NO assays. Microglia were added to mature OLs for 24 h before addition of Th1 or Th17 cells.

EAE induction

Male C57BL/6 mice (8–10 wk old) were induced with EAE using 50 μg MOGp and 125 μg desiccated *Mycobacterium tuberculosis* H37Ra (DIFCO Laboratories, Detroit, MI) emulsified in IFA, as well as i.p. injections of 200 ng *Bordetella pertussis* toxin (List Biological Laboratories, Campbell, CA) in PBS on days 0 and 2, as previously described (24, 25). For SJL mice, 9-wk-old females were induced with EAE using 150 μg proteolipid protein $(PLP)_{139–151}$ (HSLGKWLGHPDKF; CPC Scientific, San Jose, CA) and 500 μg desiccated *M. tuberculosis* H37Ra (DIFCO Laboratories) emulsified in IFA, as described (26). Mice were monitored and scored daily for signs of EAE using the following clinical scoring criteria: 0) no symptoms, 1) loss of tail tone, 2) flaccid tail, 3) partial hind limb paralysis, 4) complete hind limb paralysis, 5) moribund state (humanely euthanized), and 6) death. For C3H/HeSnJ and C3H/HeSnJ-Slc7a11$^{sut/sut}$ mice, 9-wk-old females were induced with EAE using 100 μg $PLP_{190–209}$ (SKTSASIGSLCADARMYGVL) (CPC Scientific) and 400 μg desiccated *M. tuberculosis* H37Ra (DIFCO Laboratories) emulsified in IFA, as well as i.p. injections of 400 ng *B. pertussis* toxin (List Biological Laboratories) in PBS on days 0 and 2, as described (27). Signs of atypical/rotary EAE were assessed, as previously described (28): 0) no symptoms, 1) head turned slightly, 2) head turning more pronounced/poor righting ability, 3) inability to walk in a straight line, 4) laying on side, 5) rolling continuously unless supported (humanely euthanized), and 6) death. Animals were terminated at the peak of disease.

Sulfasalazine and (S)-4-carboxyphenylglycine treatment

Mice were treated with 0.15 g/kg sulfasalazine (SAS; Sigma-Aldrich) in 0.5 ml PBS (pH 7.4) twice daily or 0.010 g/kg (*S*)-4-carboxyphenylglycine (S-4-CPG; Tocris, Minneapolis, MN), in 0.250 ml PBS (pH 7.4) twice daily by i.p. injection. Treatments were 7 h apart (19).

Flow cytometry

Mononuclear cells were isolated by a Percoll gradient (70/40). Isolated cells were either stained immediately or restimulated for T cell cytokine analysis

with 50 ng/ml PMA and 750 ng/ml ionomycin in the presence of Golgi Plug (BD Biosciences, San Jose, CA) for 4 h. Single-cell suspensions from spinal cord or spleen cells were incubated with Fc Block (2.4G2), and the following Abs were used, as appropriate: anti-CD4 (RM4-5; BD Biosciences); anti-Foxp3 (FJK-16s), anti–IFN-γ (XMG1.2), anti–IL-17A (eBio17B7), and anti–Ki-67 (SolA15) all from eBioscience (San Diego, CA). Cell viability was determined by staining with Live/Dead Fixable Near-IR Dead Cell Stain Kit (Life Technologies, Grand Island, NY). To evaluate system $_{Xc}^-$ expression on immune cells, cells were incubated with Fc Block (2.4G2), and then surface stained using anti-CD11b (M1/70) and CD45 (30-F11) (all from eBioscience), followed by intracellular staining for system $_{Xc}^-$ (Abcam, Cambridge, MA; ab37185). Cell viability was again determined by staining with Live/Dead Fixable Near-IR Dead Cell Stain Kit (Life Technologies). Stained cells were run on a LSR II Flow Cytometer (BD Biosciences) and analyzed by FlowJo (Tree Star).

Evaluation of splenocytes

Single-cell suspensions of splenocytes isolated from immunized mice were unstimulated or restimulated with either anti-CD3 (145-2C11; 1.0 μg/ml) or $MOG_{35–55}$ peptide (1.0 or 10.0 μg/ml) for 3 d. The frequency of splenocytes in cycle was measured by pulse-labeling cells with 5-ethynyl-2′-deoxyuridine (EdU; 10 μM) for 60 min before analyzing EdU incorporation using the Click-iT EdU Flow Cytometry Assay Kit (Invitrogen Molecular Probes) and live/dead staining, as previously described (24).

NO assay

Conditioned media from each experimental condition was collected and analyzed for NO production using the Nitrate/Nitrite Fluorometric Assay Kit, per the manufacturer's instructions (780051; Cayman Chemical, Ann Arbor, MI).

Glutamate assay

Conditioned media from each experimental condition was collected and analyzed for glutamate concentration using the Glutamate Assay Kit per the manufacturer's instructions (ab83389; Abcam).

Immunoblotting

Cells or tissue from whole spinal cord were lysed in a 0.1 M $NaPO_4$ buffer containing 10% SDS, a Mini Protease Inhibitor Cocktail Tablet (Roche, Indianapolis, IN), and 1% Phosphatase Inhibitor Cocktails 2 and 3 (Sigma-Aldrich). A dendritic cell protein assay (Bio-Rad, Hercules, CA) was used to measure protein concentrations. Protein lysates (8–15 μg) were resolved by electrophoresis on 10% polyacrylamide gels, transferred to polyvinylidene fluoride membranes, and assessed for protein expression (22). Rabbit anti-xCT (1:2,000; Abcam, ab37185) was used to detect the substrate-specific L chain of system $_{Xc}^-$. For detection of inducible NO synthase (iNOS), rabbit anti-iNOS (1:5,000; BD Biosciences, 610332) was used. Goat anti-actin (1:15,000; Santa Cruz Biotechnology, sc-1616) or mouse anti–β-actin (C4) HRP (Santa Cruz Biotechnology; sc-47778) were used as loading controls. Secondary Abs from Santa Cruz Biotechnology were used at concentrations of 1:4,000 (goat anti-mouse IgG-HRP, sc-2055) and 1:5,000 (goat anti-rabbit IgG-HRP, sc-2054; donkey anti-goat IgG-HRP, sc-2020). Membranes were developed using GE ECL Plus Western Blotting Detection Reagents (GE Healthcare, Buckinghamshire, U.K.) or Pierce ECL 2 Western blotting substrate (Thermo Fisher Scientific, Waltham, MA), and then exposed on HyBlot CL autoradiography film (Denville, South Plainfield, NJ) or Amersham Hyperfilm ECL (GE Healthcare, Buckinghamshire, U.K.). Films were scanned using an EPSON Perfection V33 Scanner with EPSON Scan software at 300 dots per inch, and densitometric analysis was performed using NIH ImageJ software. Densities are expressed as a ratio of the protein of interest divided by expression of the loading controls actin.

Perfusion and preparation of mouse brains and spinal cords

Spinal cords from C57BL/6 mice and SJL mice and brains from SJL mice were removed after transcardiac perfusion with 4% PFA in PBS. After perfusion, brains were fixed overnight, cryopreserved in 30% sucrose, flash frozen in OCT (Tissue Tek), and cut at 16 μm. Spinal cords were postfixed 48–72 h in 4% PFA and decalcified in 0.003 M EDTA and 1.35 M HCL for 24 h. Spinal cords were then cut into 2-mm sections, embedded in paraffin, and cut at 5 μm.

Luxol fast blue staining

Global changes in myelin were assessed by Luxol fast blue. Quantification included the extent of demyelination according to the proportion of white matter affected: 0, 1, 2, 3, or 4 for none; ∼25%, ∼50%, ∼75%, or ∼100%, respectively. For C57BL/6 spinal cord assessments, seven sections from thoracic, lumbar, and sacral regions of the spinal cord from each animal were analyzed. For SJL brain assessments, four to six sections of the corpus callosum at the level of the anterior hippocampus were assessed.

Immunohistochemistry of brain and spinal cord sections

Ag retrieval was performed using 10 mM citrate buffer (pH 3 or 6), with boiling for 20 min. For diaminobenzidine (DAB) staining, slides were incubated in 0.3% hydrogen peroxide in methanol to block endogenous peroxidase activity. Sections were blocked in 5% serum corresponding to the host of the secondary Ab with 0.3% Triton X-100 for 1 h at room temperature. Primary Abs were diluted in blocking buffer and incubated on sections overnight at 4°C. Secondary Abs were diluted in blocking buffer and incubated on sections for 1 h at room temperature. For DAB staining, a Tyramide Signal Amplification Kit (Perkin Elmer, Waltham, MA) was used with the Vectastain ABC Kit (Vector Laboratories, Burlingame, CA), and a Peroxidase Substrate Kit (Vector Laboratories, Burlingame, CA). Slides used for DAB staining were dehydrated and mounted with Permount (Fisher Scientific, Waltham, MA). For fluorescent staining, slides were mounted with Fluoromount-G (Southern Biotech, Birmingham, AL). Mouse anti–glial fibrillary acidic protein (GFAP; 1:1000; Sigma-Aldrich, SAB2500462) was used to evaluate expression of astrocytes. Rabbit anti-Iba1 (1:1000; Wako, 019-19741) or goat anti-Iba1 (1:100; Abcam, ab107159) was used to evaluate expression of microglia and macrophages. Rabbit anti-xCT (1:100; Abcam, ab37185) was used to evaluate expression of the system $_{Xc}^-$ transporter. Secondary Abs for immunofluorescence included Alexa Fluor 594 goat anti-mouse IgG (1:1000; Invitrogen, A11032), Alexa Fluor 488 goat anti-rabbit IgG (1:1000; Invitrogen, A11043), and rhodamine (tetramethylrhodamine isothiocyanate)-conjugated donkey anti-goat (1:200; Jackson ImmunoResearch, 705025003). Secondary Abs for DAB staining included biotinylated anti-mouse (1:200; Vector Laboratories, BA-2000) and biotinylated anti-rabbit (1:200; Vector Laboratories, BA-1000).

Imaging

Confocal images were captured using a Leica TCSSP5 laser-scanning confocal microscope. The Leica LASAF software and Adobe Photoshop (for contrast, brightness, and color adjustments) were used to create figures and process images. Phase-contrast images for cell cultures were captured using a Nikon TI-U inverted microscope using NIS-Elements software (Melville, NY).

Quantification of GFAP, Iba-1, and system $_{Xc}^-$ staining in spinal cord and brain sections

For quantification of GFAP, Iba-1, and system $_{Xc}^-$ staining in spinal cord sections, fluorescent images were acquired using an Olympus BX51 microscope (Olympus America, Melville, NY) with 4×, 0.13 NA lens, and Stereo Investigator software (version 11.04; MBF Bioscience, Williston, VT). Cellular staining in thoracic and lumbar sections was analyzed (Image J software; 1.48v) using the area fraction technique (29). Briefly, images were de-noised using rolling-ball background subtraction. The threshold was set to the same baseline across experimental groups for each Ab to measure area of cellular staining. All assessments were made from six sections from thoracic and lumbar regions of the spinal cord from each animal. For quantitative analyses of GFAP- and Iba-1–immunopositive cells in SJL mouse brains, DAB-stained bright field images were acquired using an Olympus BX51 microscope (Olympus America) with 20×, 0.50 NA lens, and Stereo Investigator software (version 11.04; MBF Bioscience). Three adjacent sections, each in three regions of the brain (approximately bregma −0.10 mm, −1.70 mm, and −2.30 mm), were used for a total of nine sections per animal. Cell bodies in a 214 μm × 142-μm region of the corpus callosum and cingulum bundle were counted in the left and right hemispheres, and these numbers averaged to obtain a count of cells per mm^2 tissue.

Statistical analysis

All statistical analyses were performed using GraphPad Prism software version 5.03 (GraphPad Software, La Jolla, CA). Specific analyses performed including p values are reported where indicated.

Results

System $_{Xc}^-$ transporter inhibitors attenuate experimental autoimmune encephalomyelitis

System $_{Xc}^-$ is an important glutamate release mechanism in oxidizing environments that may contribute to excitotoxic mecha-

nisms in autoimmune demyelination. System $_{Xc}^-$ transporter expression is upregulated in spinal cords of C57BL/6 mice with EAE (Supplemental Fig. 1) (30). We tested the effect of treating EAE in C57BL/6 mice with the system $_{Xc}^-$ transporter inhibitor SAS. Treatment with SAS was initiated 7 d after immunization with MOGp. EAE was significantly less severe in C57BL/6 mice treated with SAS versus mice treated with PBS (Fig. 1A). Luxol fast blue staining of spinal cords demonstrated reduced demyelination in EAE mice treated with SAS compared with EAE mice treated with PBS (Fig. 1B). Additionally, mice treated with S-4-CPG, an inhibitor of the system $_{Xc}^-$ transporter with no known effect on NF-κB (19), also demonstrated significantly reduced clinical disease (Fig. 1C) that was associated with decreased demyelination (Fig. 1D). These data provide evidence that inhibiting the system $_{Xc}^-$ transporter attenuates clinical disease consistent with a reduction in demyelination.

Evaluation of markers for specific inflammatory cell types by immunofluorescent staining demonstrated an increase in reactive astrocytes (GFAP) and activated microglia (Iba-1) in EAE (Fig. 2A, *middle panels*) compared with control (unimmunized) mice (Fig. 2A, *left panels*). In SAS-treated mice, the expression of GFAP and Iba-1 (Fig. 2A, *right panels*) was reduced to levels equivalent to control mice (quantification is reported in Fig. 2B, 2C, respectively). The expression of system $_{Xc}^-$ was also elevated in PBS-treated EAE spinal cords (Fig. 2A, *middle panel*) compared with control mice (Fig. 2A, *left panel*). In SAS-treated mice, the expression of system $_{Xc}^-$ (Fig. 2A, *right panel*) was reduced to levels equivalent to control mice (Fig. 2A, *left panel*). Quantification of system $_{Xc}^-$ staining is reported in Fig. 2D. The system $_{Xc}^-$ transporter colocalized with reactive microglia (Fig. 3) in gray and white matter from spinal cords subjected to EAE. These data indicate that the increase in system $_{Xc}^-$ expression in EAE spinal cords is due in part to an increase in system $_{Xc}^-$ transporter expression in reactive microglia.

Reduced immune cell infiltration into the spinal cords of SAS-treated EAE mice

To determine whether the CNS protection observed in SAS-treated EAE mice is a result of reduced peripheral immune cell migration into the CNS, spinal cords were analyzed for altered inflammatory cell populations 15 d after immunization (i.e., peak of disease). Representative dot plots (Fig. 4A) demonstrate a reduction in overall number of $CD4^+$ infiltrating T cells in spinal cords from SAS-treated mice compared with spinal cords from PBS-treated mice (numbers in *upper right quadrants*). IFN-γ^+, IL-17^+, and $Foxp3^+$ were also reduced (Fig. 4B). Although there is a statistically significant reduction in $CD4^+$, IFN-γ^+, IL-17^+, and $Foxp3^+$ T cells in the spinal cord (Fig. 4B), the proportion of infiltrating IFN-γ^+ IL-17^+, IFN-γ^+ IL-17^-, IL-17^+ IFN-γ^-, and T $regulatory^+$ cells remained unchanged between PBS- and SAS-treated mice (Fig. 4C). These data suggest a role for system $_{Xc}^-$ in regulating immune cell infiltration into the CNS. Therefore, we next evaluated the expression of system $_{Xc}^-$ on infiltrating immune cells of peripheral origin. System $_{Xc}^-$ expression on peripheral CNS-infiltrating immune cells, including $CD45^{high}CD11b^{low}$ lymphoid cells, which are predominantly T cells, as well as $CD45^{high}CD11b^{high}$ macrophages was comparable with expression on CNS microglia ($CD45^{int}CD11b^{high}$) from EAE spinal cord lysates (Fig. 4D).

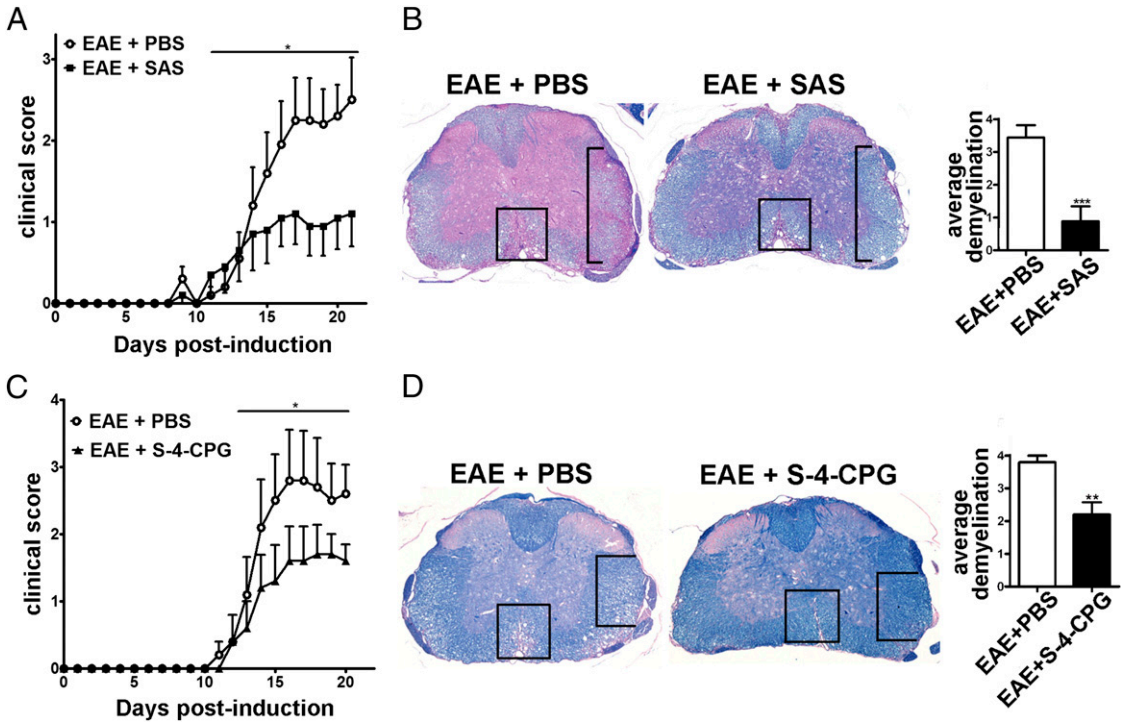

FIGURE 1. Pharmacological blockade of the system $_{Xc}^-$ transporter attenuates EAE. (**A**) EAE clinical scores (mean ± SEM) of C57BL/6 mice treated with PBS ($n = 20$) or SAS ($n = 19$) from day 7 postimmunization with MOGp. Data are from three pooled independent experiments. (**B**) Luxol fast blue immunohistochemistry of spinal cords from EAE mice treated with PBS and SAS. Representative areas of demyelination are in boxed or bracketed regions. Quantitation of demyelination (mean ± SEM, $n = 8$ mice from each group, six sections per mouse). (**C**) EAE clinical scores (mean ± SEM) of C57BL/6 mice treated with PBS ($n = 5$) or S-4-CPG ($n = 5$) from day 7 postimmunization with MOGp. (**D**) Luxol fast blue immunohistochemistry of spinal cords from EAE mice treated with PBS and S-4-CPG. Representative areas of demyelination are in boxed or bracketed regions. Quantification of demyelination (mean ± SEM, $n = 5$ mice from each group, six sections per mouse). Statistical differences for (A) and (D) were determined using a nonparametric two-tailed Mann–Whitney U test; top line represents values used to determine statistical measures. Two-tailed t test was used for all bar graphs. $^*p < 0.05$, $^{**}p < 0.01$, $^{***}p < 0.001$.

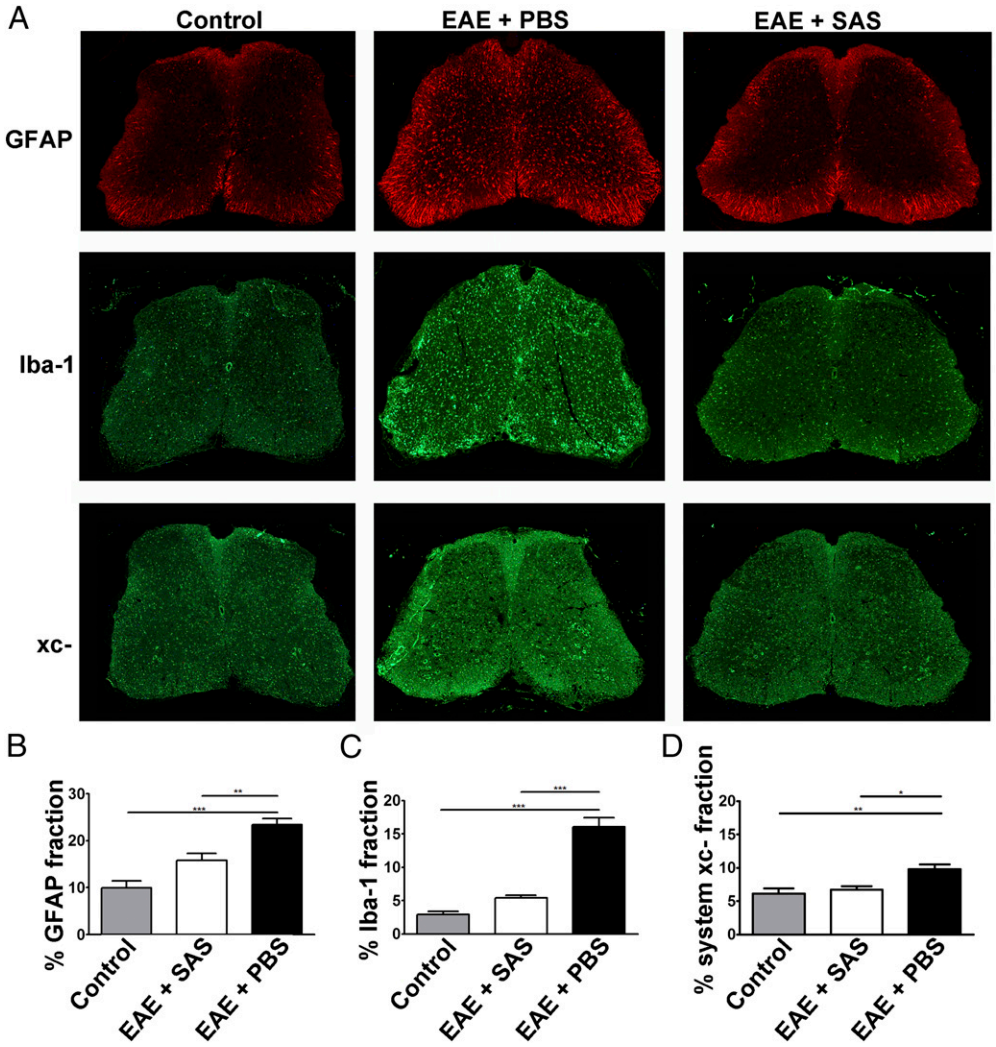

FIGURE 2. Reactive glia are reduced in EAE mice treated with SAS. (**A**) Fluorescent labeling for GFAP, Iba-1, or system $_{Xc}^{-}$ in the spinal cord of control (unimmunized) mice (*left panels*) and EAE mice treated with PBS (*middle panels*) or SAS (*right panels*). Quantification of staining was determined by measuring area of mean fluorescent staining for GFAP (**B**), Iba-1 (**C**), and system $_{Xc}^{-}$ (**D**). Mean ± SEM, $n = 3$ control, three SAS-treated, or four PBS-treated mice, six sections per mouse. Statistical differences were determined using a one-way ANOVA, $*p < 0.05$, $**p < 0.01$, $***p < 0.001$.

SAS also inhibits NF-κB (31), and therefore low numbers of inflammatory cells in the spinal cord may be a result of poor activation of T cells in the periphery. To test for this, the proportion of $CD4^+$ T cells, as well as IFN-γ^+, IL-$17A^+$, and $Foxp3^+$ cells, was assessed in spleens from PBS- and SAS-treated mice, and no statistical difference was observed (Fig. 5A). Additionally, the percentage of proliferating cells in spleens from PBS- and SAS-treated mice detected by labeling with Ki-67 showed no statistically significant change (Fig. 5B, *left panel*; representative dot plots, *right panels*). Ki-67^+ staining in naive mouse spleens demonstrated that 10% of $CD4^+$ cells were proliferating, similar to published results (32). This suggests that there is a 2- to 3-fold increase in proliferation as a consequence of EAE. To further evaluate T cell activation in the periphery, spleen cells from SAS- and PBS-treated mice were restimulated with 1 μg/ml MOGp or anti-CD3 and 10 μg/ml MOGp. Proliferation was assessed by the EdU pulse incorporation assay (24). Representative dot plots (Fig. 5C, *left panel*) demonstrate little change in the proportion of proliferating cells (numbers in *lower right quadrants*), which is not statistically significant (Fig. 5C, bar graphs). These results show that the precursor frequency of peripheral MOGp-reactive T cells and ability to enter into the cell cycle were not affected by SAS treatment. We therefore conclude that low numbers of infiltrating inflammatory cells in the CNS of SAS-treated mice are not due to compromised activation of MOGp T cells in the periphery.

Mice lacking functional system $_{Xc}^{-}$ are resistant to EAE

To further corroborate the role of system $_{Xc}^{-}$ in modulating autoimmune encephalomyelitis, we evaluated the development of EAE in mice deficient in system $_{Xc}^{-}$ function (C3H/HeSnJ-Slc7a11$^{sut/sut}$) and wild-type littermate controls (C3H/HeSnJ$^{+/+}$). C3H/HeSnJ-Slc7a11$^{sut/sut}$ mice harbor a loss of function mutation

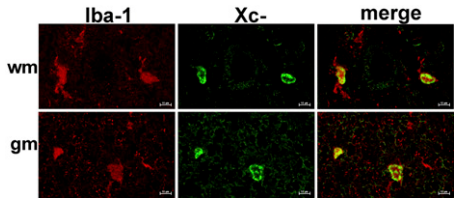

FIGURE 3. The system $_{Xc}^{-}$ transporter colocalizes with microglia, macrophages, and T cells in PBS-treated EAE mouse spinal cords. Confocal imaging of fluorescently labeled Iba-1, system $_{Xc}^{-}$ transporter, and merge in mouse spinal cord white matter (wm) or gray matter (gm) from PBS-treated C57BL/6 EAE mice subjected to EAE. Images are representative of six sections each from $n = 3$ mice PBS treated. Scale bars, 15 μm.

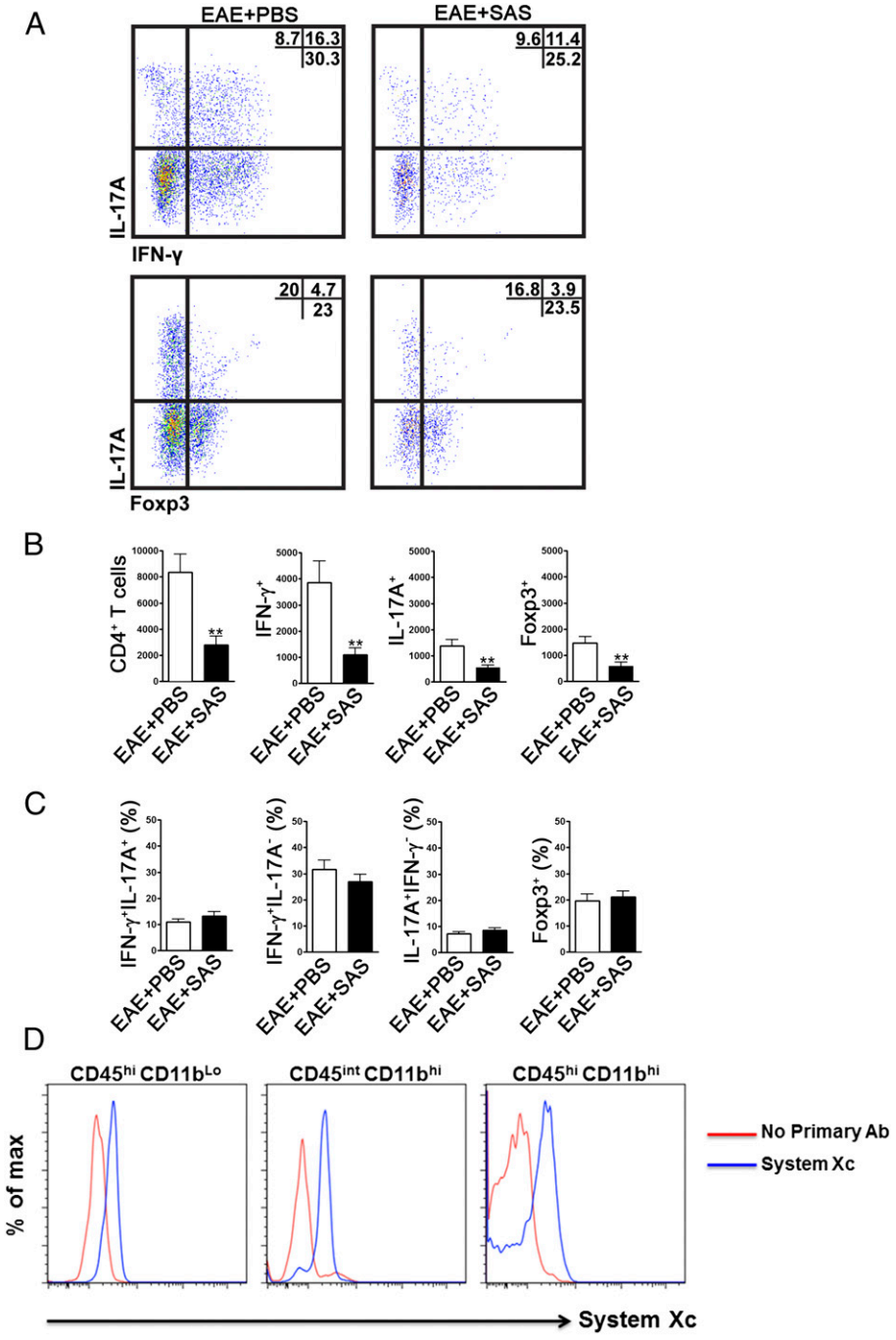

FIGURE 4. Reduced T cell infiltration into the spinal cord of EAE mice treated with SAS. C57BL/6 mice were treated with SAS or PBS, beginning 7 d post-induction of EAE. Spinal cords were obtained on day 15. (**A**) Representative dot plots show Th1 (IFN-γ^+/IL-17^-) and Th17 (IFN-γ^-/IL-17^+) cells in $CD4^+$ gate (*upper panels*) and T regulatory cells ($Foxp3^+$) (*lower panels*). Dot plots show percentages in *upper right quadrant*. (**B**) Absolute numbers of $CD4^+$ cells as well as IFN-γ^+, IL-$17A^+$, and $Foxp3^+$ cells were statistically analyzed. (**C**) The change in percentage of T cell populations between SAS- and PBS-treated EAE mice was also examined. Mean ± SEM, $n = 10$ for PBS treated, and $n = 9$ for SAS treated from two independent experiments. Two-tailed t test was used for all bar graphs. $^{**}p < 0.01$. (**D**) FACS analysis of system $_{Xc}^-$ transporter expression in spinal cord single-cell suspensions from PBS-treated EAE mice stained with $CD45^{high}CD11b^{low}$ (lymphocytes, mainly T cells), $CD45^{int}CD11b^{high}$ (microglia), and $CD45^{high}CD11b^{high}$ (macrophages). Images are representative of $n = 10$ mice from two independent experiments. System $_{Xc}^-$ transporter staining (blue line) is compared with no primary Ab (red line).

in the Slc7a11 gene that encodes for the system $_{Xc}^-$ L chain in the C3H/HeSnJ background (33). EAE in C3H/HeSnJ$^{sut/sut}$ mice was significantly attenuated and delayed compared with C3H/HeSnJ$^{+/+}$ littermates (Fig. 6A). The incidence of disease was 60% in the C3H/HeSnJ$^{+/+}$ compared with 20% in C3H/HeSnJ$^{sut/sut}$ mice (Fig. 6B). The average incidence of EAE in C3H/HeJ mice immunized with $PLP_{190–209}$ is 50% (27). $CD4^+$ T cells responding to $PLP_{190–209}$ in a recall assay were similar between C3H/HeSnJ$^{+/+}$ and C3H/HeSnJ$^{sut/sut}$ mice (data not shown). These data support the pharmacological evidence that the system $_{Xc}^-$ transporter plays an important role in the pathogenesis of EAE.

SAS attenuates relapsing-remitting EAE

The SJL mouse immunized with the $PLP_{139–151}$ peptide develops a relapsing-remitting form of EAE that clinically reflects human relapsing-remitting MS (34). To test whether a system $_{Xc}^-$ inhibitor could ameliorate relapsing-remitting EAE, SAS treatment in SJL mice with EAE was initiated on day 24 postimmunization during the first relapse after T cell infiltration into the CNS has occurred. We observed that clinical symptoms associated with EAE were significantly diminished in SAS-treated mice compared with PBS-treated controls (Fig. 7A). The recovery from EAE in SAS-treated mice was associated with reduced demyelination in the spinal cord (Fig. 7B). Brain pathology as well as spinal cord pathology occurs in SJL mice induced with EAE (34). As such, inflammation and myelin degradation in the corpus callosum and overlying cortex were also assessed in SJL mice when SAS treatment was initiated during an EAE relapse on day 24 post-immunization. The brains of SAS-treated mice had fewer activated microglia (Iba-1; Fig. 8, *top row*) and reactive astrocytes

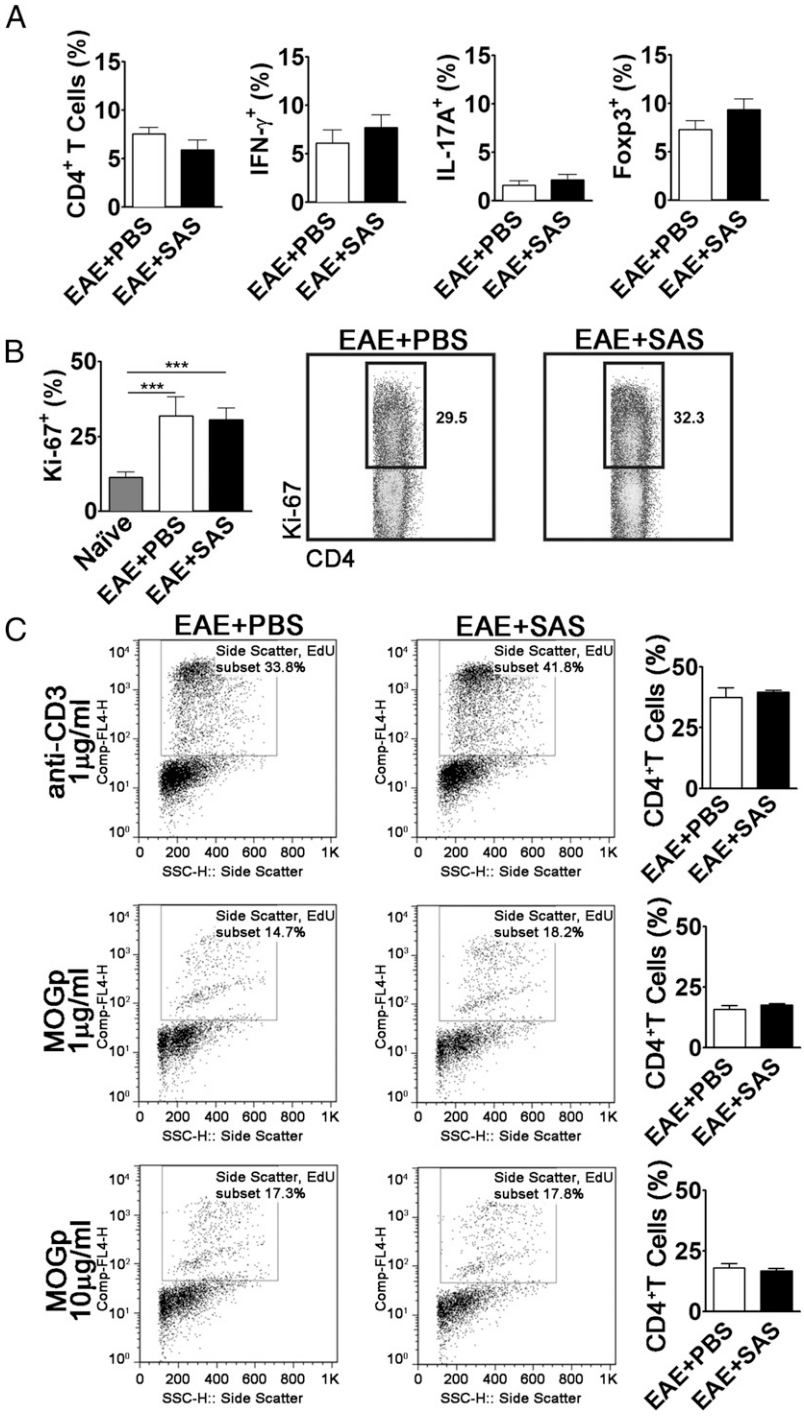

FIGURE 5. MOG-responding T cells in the periphery are equivalent in PBS- and SAS-treated EAE mice. Spleens from PBS- and SAS-treated mice were analyzed 15 d postinduction of EAE. (**A**) The percentage of $CD4^+$ T cells, Th1 (IFN-γ^+/IL-17^-), Th17 (IFN-γ^-/IL-17^+), and T regulatory cells ($Foxp3^+$) in spleens from PBS-treated ($n = 10$) and SAS-treated ($n = 9$) mice from two independent experiments. (**B**, *left panel*) The percentage of Ki-67–positive cells in the CD4 population from naive spleens ($n = 4$) as well as from PBS ($n = 5$)- and SAS-treated mice ($n = 5$) induced with EAE. A one-way ANOVA test demonstrated statistical significance between the proportion of Ki-67^+ cells from naive spleens compared with either PBS- or SAS-treated EAE spleens. No significance was observed between PBS- and SAS-treated EAE spleens. (B, *right panel*) Representative dot plots; numbers indicate proportion of proliferation. (**C**) Proportion of cells entering into the cell cycle in response to anti-CD3 or MOGp measured by 1-h EdU uptake assay in spleens from EAE mice treated with PBS ($n = 6$) or SAS ($n = 6$). Dot plots show percentages. Bar graphs represent two-tailed t test. $^{***}p < 0.001$.

(GFAP; Fig. 8, *middle row*), which was consistent with a reduction in myelin damage (luxol fast blue; Fig. 8, *bottom row*) compared with PBS-treated mice. These data provide evidence that SAS modulates disease pathology in the forebrain of SJL mice after immune cell infiltration into the CNS.

SJL mice treated with SAS before onset of clinical symptoms (from day 7 postimmunization) developed no clinical symptoms of EAE (data not shown). Overall, these results show that inhibition of the system $_{Xc}^-$ transporter attenuates established relapsing-remitting EAE.

Encephalitogenic Th1 but not Th17 cells promote microglia-induced death of mature OLs

Th1 and Th17 cells contribute to the pathogenesis of MS, and animal models that represent MS, by different modes of action (35, 36). To further explore how T cell infiltration into the CNS induces system $_{Xc}^-$ expression, glutamate release, and excitotoxicity to myelin, we used a coculture model of MOG-specific Th1 and Th17 cells with primary microglia and mature myelin protein–producing OLs. T cells from MOGp-immunized mice were cultured under polarizing conditions to generate MOG-reactive Th1 and Th17 cells, respectively (Supplemental Fig. 2). Both Th1 and Th17 cells expressed TNF-α (data not shown). Th1 and Th17 cells were cocultured with mature OLs (identified as myelin basic protein–expressing cells) in the presence and absence of microglia for 48 h to determine their effects on mature OL viability. Coculture of encephalitogenic Th1 cells or microglia with mature OLs did not significantly reduce the number of OLs, as quantified by Olig2 staining, a specific marker for OLs (Fig. 9A). However, we observed

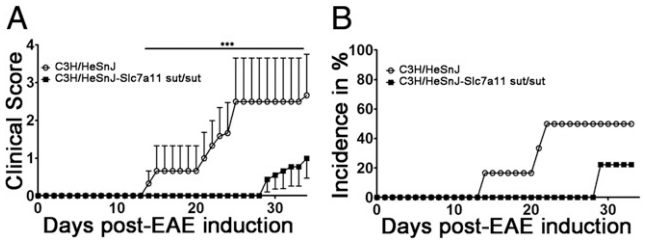

FIGURE 6. Mice lacking functional system $_{Xc}^{-}$ are resistant to EAE. (**A**) Mean clinical scores of EAE in C3H/HeSnJ$^{+/+}$ (n = 6) and littermate C3H/HeSnJ$^{sut/sut}$ mice (n = 9). Two-tailed nonparametric Mann–Whitney U test, mean ± SEM, ***$p < 0.0001$. (**B**) Incidence of EAE.

a significant decrease in number of mature OLs if both microglia and Th1 cells were present in the cocultures (Fig. 9A). In contrast to Th1 cells, Th17 cells in the absence of microglia were sufficient to induce a significant decrease in mature OL number that was not further reduced in the presence of microglia (Fig. 9B). These results demonstrate that MOG-specific CD4$^+$ Th1-induced death of mature OLs is microglia dependent, whereas MOG-specific CD4$^+$ Th17 cells can directly promote death of mature OLs.

Th1 but not Th17 cells induce NO release from microglia that is inhibited by Abs against TNF-α + IFN-γ

A mechanism by which microglia can induce death to OLs is NO production. Th1 and Th17 cells were next tested for their ability to induce NO release from microglia. We cocultured Th1 or Th17 cells with mature OLs in the absence or presence of microglia for 48 h, after which supernatants were tested for NO. Mature OLs did not express NO (Fig. 9C, 9D), consistent with their lack of iNOS (37). Microglia cocultured with mature OLs also did not express NO (Fig. 9C). Th1 cells produced NO that was further increased in the presence of microglia (Fig. 9C). In contrast, Th17 cells did not produce NO even in the presence of microglia (Fig. 9C). To determine whether NO produced by Th1 and potentiated in the presence of microglia was dependent on the cytokines produced by Th1 signaling, neutralizing Abs to IFN-γ and TNF-α (I+T) were added to cocultures. Anti–IFN-γ and anti–TNF-α reduced NO production from Th1 cells as well as Th1-potentiated NO release from microglia (Fig. 9D). We conclude that MOG-specific Th1 cells, but not Th17 cells, produce NO and potentiate NO release from microglia that is dependent on IFN-γ and TNF-α signaling.

Th1 but not Th17 cytokines induce NO release from microglia and subsequent mature OL death

Th1 cells produce IFN-γ, and Th17 cells produce IL-17A and IL-17F. Both Th1 and Th17 cells produce TNF-α (38). To determine whether these cytokines produced by Th1 cells activate microglia to promote mature OL death, microglia were cocultured with mature OLs in the presence of 100 ng/ml IFN-γ or TNF-α alone or in combination for 48 h. IFN-γ reduced mature OL number that was not further enhanced by addition of IL-17A or IL-17F (Fig. 10A, 10B). Addition of TNF-α alone did not induce mature OL death (Supplemental Fig. 3A, 3B). However, if both IFN-γ and TNF-α were added to the cultures, almost all mature OLs were killed (Fig. 10B). IFN-γ and TNF-α led to significant production of NO, whereas all other cytokines individually or in combination did not (Fig. 10C). Treatment of microglia/OL cocultures with the Th17 cytokines IL-17A or IL-17F alone or in combination with each other did not cause OL death (Supplemental Fig. 3A, 3B) nor increase NO production (Fig. 10C). No combination of cytokine treatment in the absence of microglia induced mature OL death (data not shown).

In the experiments above, MOGp-expanded Th1 and Th17 cells were of mouse origin, whereas mature OLs and microglia were from rat (Fig. 10). Because the mechanism by which Th1 and Th17 cells induce death of mature OLs is strikingly different, an allogeneic response does not appear to be a confounding factor in our interpretation. To further limit this possibility, the effect of murine cytokines on rat mature OL and microglia cocultures was tested. We again observed that treatment with IL-17A, IL-17F, and TNF-α (100 ng/ml each for 48 h) alone or in combination did not cause death of or induce production of NO (Supplemental Fig. 3C). IFN-γ treatment was toxic to OLs, and combined treatment with murine IFN-γ and TNF-α further significantly reduced mature OL number (Supplemental Fig. 3B). As with rat cytokines only IFN-γ and TNF-α induced the production of NO from microglia. These results provide evidence that the cytokines produced from MOGp-expanded Th1 cells potentiate death of OLs in the presence of microglia.

iNOS inhibitors block death of mature OLs induced by cytokine-activated microglia

We used inhibitors of iNOS to directly test whether production of NO by microglia after exposure to Th1-associated cytokines caused death to mature OLs. Microglia/Mature OL cocultures were pretreated with iNOS inhibitor 1400W before exposure to IFN-γ and TNF-α (100 ng/ml each) for 48 h. IFN-γ– and TNF-α–stimulated microglia caused significant death to mature OLs that was blocked by 1400W (Fig. 11A, 11B). Similar results were observed with aminoguanidine, another inhibitor of iNOS (data not shown). Western immunoblotting of lysate from microglia unstimulated or stimulated with IFN-γ and TNF-α resulted in a 7.5-fold increase in iNOS expression (Fig. 11C). These data indicate that cytokines associated with Th1 signaling induce NO release from microglia and cause death of mature OLs.

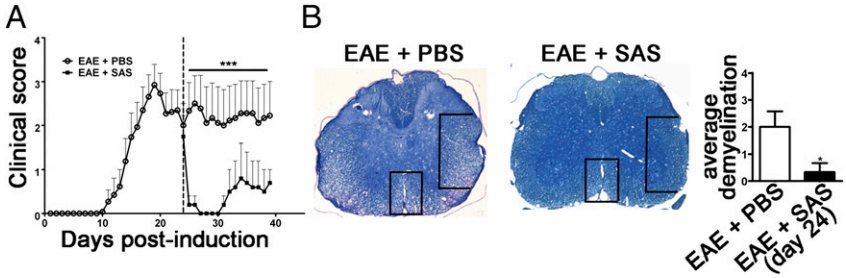

FIGURE 7. SAS attenuates relapsing-remitting EAE. (**A**) EAE in SJL mice immunized with PLP peptide treated with PBS (n = 8) or SAS (n = 8) from day 24 postinduction (dashed line). Data are mean ± SEM of clinical scores. Statistical difference was determined using a nonparametric two-tailed Mann–Whitney U test. Top line represents values used for statistical analysis. (**B**) Luxol fast blue immunohistochemistry of spinal cords from EAE mice treated with PBS and SAS. Representative areas of demyelination are in boxed or bracketed regions. Quantitation of demyelination (mean ± SEM, n = 3 mice from each group, six sections per mouse). Two-tailed t test was used for bar graph. *$p < 0.05$, ***$p < 0.001$.

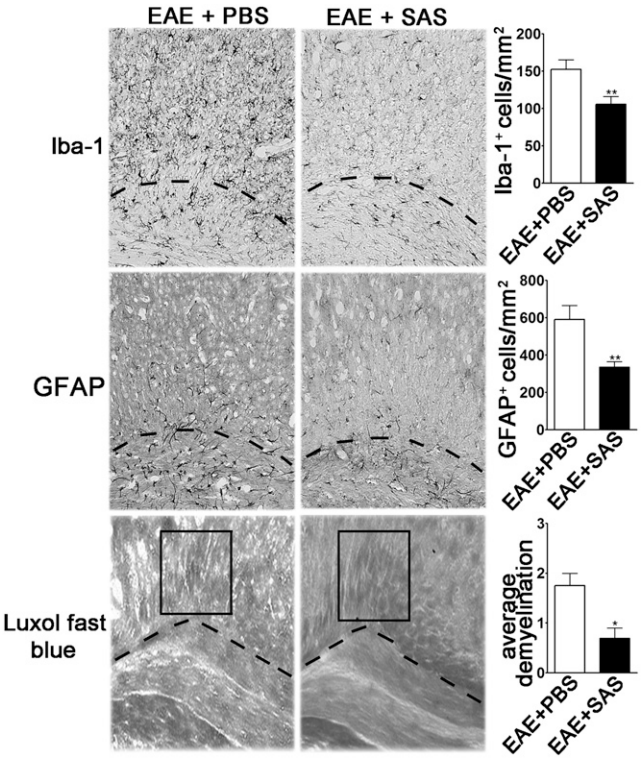

FIGURE 8. SAS reduces expression of reactive glia in corpus callosum and overlying cortex in relapsing-remitting EAE. *Top panels*, DAB labeling for Iba-1 in brains from SJL EAE mice treated with PBS (*left panel*) or SAS (*right panel*). *Middle panels*, DAB labeling for GFAP in brains from SJL EAE mice treated with PBS (*left panel*) or SAS (*right panel*). *Bottom panels*, Luxol fast blue immunohistochemistry of brains from SJL EAE mice treated with PBS (*left panel*) and SAS (*right panel*). Area under the dotted curve is corpus callosum. Boxed regions represent area quantified. Boxed regions in luxol fast blue staining highlight demyelination of axons from the corpus callosum projecting into layer six of the cerebral cortex. Quantitation (mean ± SEM, $n = 3$ mice from each group, six sections per mouse). Two-tailed t test, $^{*}p < 0.05$, $^{**}p < 0.01$.

IFN-γ– and TNF-α–stimulated microglia induce excitoxicity in mature OLs

High concentrations of NO can result in energy failure, leading to release of glutamate and subsequent excitotoxicity in neurons (39–41). We tested whether mature OL death induced by IFN-γ– and TNF-α–stimulated microglia involves an excitotoxic component. Mature OL/microglia cocultures were pretreated with either an AMPA receptor antagonist (NBQX, 100 μM) or a *N*-methyl-D-aspartate (NMDA) receptor antagonist (MK801, 10 μM) for 1 h prior to addition of IFN-γ and TNF-α for 12 h. Pretreatment with NBQX significantly rescued mature OL death. However, pretreatment with MK801 was not significantly protective (Fig. 12A, 12B). These data indicate that excitotoxicity of mature OLs induced by IFN-γ– and TNF-α–stimulated microglia is mediated by AMPA receptors, but not NMDA receptors.

Inhibitors of the system $_{Xc}^{-}$ transporter protect mature OLs from excitotoxicity

Release of glutamate from the system $_{Xc}^{-}$ transporter is a well-known source of glutamate toxicity during energy failure (16, 21, 42, 43). The system $_{Xc}^{-}$ transporter imports L-cystine into the cell to be used in the metabolism of glutathione, an important antioxidant. In exchange for the import of L-cystine, the system $_{Xc}^{-}$ transporter exports glutamate (16, 44). We found that expression of the system $_{Xc}^{-}$ transporter was elevated in IFN-γ– and TNF-α–treated microglia (Fig. 12C). IFN-γ– and TNF-α–stimulated microglia produced an increase in extracellular glutamate that was blocked by SAS, a system $_{Xc}^{-}$ inhibitor (19, 45) (Fig. 12D). Treatment with SAS in the microglia/OL inflammatory paradigm is protective to mature OLs (Fig. 12E, 12F). In addition to blocking glutamate release from the system $_{Xc}^{-}$ transporter, SAS attenuates NF-κB, a key regulator of inflammation. S-4-CPG, another inhibitor of the system $_{Xc}^{-}$ transporter that has no effect on NF-κB (16), also prevents excitotoxicity to mature OLs. These results show that glutamate release from microglia through the system $_{Xc}^{-}$ transporter contributes to excitotoxicity in mature OLs.

Discussion

These studies reveal an important link between inflammation and glutamate dysregulation in autoimmune inflammatory demyelination as well as identify the system $_{Xc}^{-}$ transporter on reactive glia as an important source of excitotoxic glutamate release. Moreover, these studies provide evidence that the system $_{Xc}^{-}$ transporter has an important role in regulating immune cell infiltration into the CNS and in the progression of autoimmune demyelination.

Our data demonstrate that myelin-specific $CD4^{+}$ Th1 and Th17 cells initiate different signaling mechanisms for myelin destruction. Th17 cells caused direct death of mature OLs, whereas Th1 cells required a mediator. Th17-induced mature OL death is independent of cytokines associated with Th17 signaling, because direct stimulation with cytokines did not result in mature OL death. Important clues for how Th17 cells may trigger mature OL death are provided by a recent in vivo imaging study demonstrating that Th17 cells make direct contact with neurons, causing increased neuronal calcium signaling (46). Th17 cells killed neurons in an in vitro coculture system, and cell death was partially blocked by NMDA receptor antagonists, suggesting a possible role for glutamate in death by Th17 cells (46).

Although NO produced by neuronal NO synthase plays an important role in neurotransmission, NO derived from iNOS is produced mainly by activated astrocytes and microglia and is not present in OLs (37, 47–49). Cytokines and/or LPS have been shown to induce NO production in microglia and astrocytes (37, 50–53). However, we demonstrate that Th1 cells can produce NO as well as potentiate NO release from microglia, unlike Th17 cells. This production of NO is contributed by TNF-α/IFN-γ signaling because neutralizing Abs to these cytokines blocked NO production. In our study, IFN-γ–stimulated microglia did cause mature OL death, which was potentiated in the presence of TNF-α. Cell death occurred presumably due to the production of NO because neither cytokine alone caused NO release from microglia. Direct cytokine exposure to mature OLs did not produce cell death. A previous study reported that direct IFN-γ exposure to OL progenitor cells induced cell death (54), most likely through activation of IFN-γ receptors located on OLs (55). The difference in these findings may be due to the fact that the OLs used in our study were fully differentiated, rather than progenitor OLs. Cytokine-stimulated production of NO from microglia also resulted in an increase in iNOS. Inhibiting iNOS protected mature OLs from TNF-α/IFN-γ–stimulated microglia, demonstrating a role for NO in triggering mature OL death. The relevance of iNOS contributing to the neuroinflammatory disease state is demonstrated in an in vivo study in which iNOS inhibitors ameliorated clinical scores in mice subjected to EAE (56).

NO production also has relevance to excitotoxic mechanisms. NO production from LPS-activated glia inhibits cellular respiration

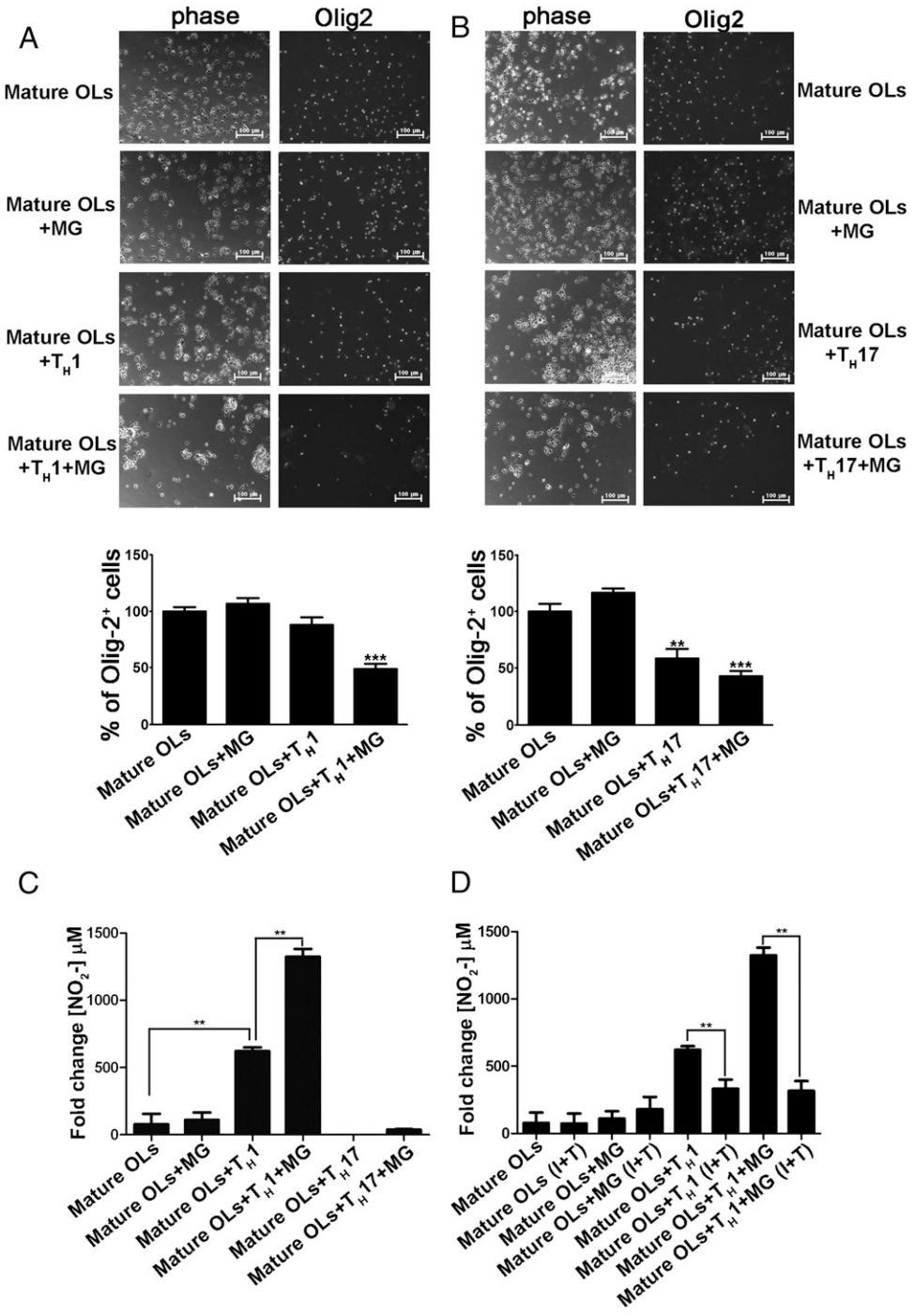

FIGURE 9. Microglia are required for MOG-specific Th1, but not Th17-mediated mature OL death. Th1 or Th17 cells were cocultured with mature OLs in the absence or presence of microglia for 48 h. Phase-contrast images and Olig2 immunocytochemistry show the mature OLs remaining after 48-h coculturing with Th1 (**A**) or Th17 (**B**) cells, in the absence or presence of microglia (MG). *Lower bar graphs* represent quantification of Olig2-positive cells in each experimental condition expressed as percentage of control of mature OLs alone (mean ± SEM from three independent experiments). Th1 cells, but not Th17 cells, induce NO release from microglia that is inhibited by Abs against TNF-α and IFN-γ. Scale bars, 100 µm. (**C**) Th1 or Th17 cells (4×10^5) were cultured with or without mature OLs and/or microglia (1×10^5) for 48 h. Changes in supernatant NO concentration as a result of coculture of mature OLs with microglia (MG) and/or T cells are shown as fold change compared with control (mature OLs; mean ± SEM, $n = 3$ independent experiments with four replicates per experiment). (**D**) Th1 (4×10^5) cells were cultured with and without mature OLs and/or microglia in the presence and absence of Abs for TNF-α and IFN-γ. Changes in supernatant NO concentration as a result of coculture of mature OLs with microglia (MG) and/or T cells with or without Abs for IFN-γ (I) and TNF-α (T) are shown as fold change compared with control (mature OLs; mean ± SEM, $n = 3$ independent experiments with four replicates per experiment). Statistical differences compared with control (mature OLs) were determined using one-way ANOVA, followed by Bonferonni multiple comparison posttest (**$p < 0.01$, ***$p < 0.001$).

causing energy failure and glutamate release in culture, resulting in neuronal NMDA glutamate receptor-mediated excitotoxicity (40, 57–59). In this work, we demonstrate that Th1-associated cytokines TNF-α and IFN-γ induce production of NO from microglia that causes AMPA glutamate receptor-mediated excitotoxicity to mature OLs. Glutamate transporters (excitatory amino acid trans-

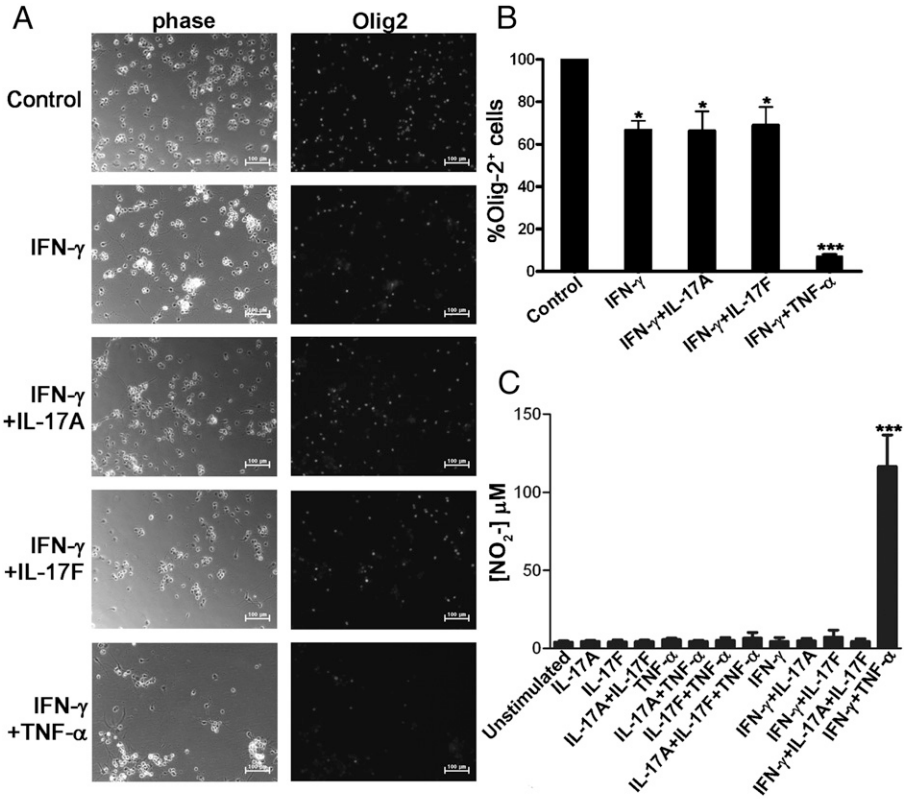

FIGURE 10. IFN-γ plus TNF-α induces death of mature OLs and production of NO in the presence of microglia. (**A**) Purified microglia (1×10^5) were plated onto mature OLs and left unstimulated or treated with 100 ng/ml IFN-γ, IFN-γ + IL-17A, IFN-γ + IL-17F, or IFN-γ + TNF-α for 48 h. Phase-contrast images and corresponding immunocytochemistry for Olig2 are shown. Scale bars, 50 μm. (**B**) Quantification of Olig2-positive cells shown in (A) expressed as percentage of unstimulated control (mean ± SEM, $n = 3$ independent experiments with four replicates per experiment). (**C**) Purified microglia (1×10^5) were plated onto mature OLs, and cocultures were treated with 100 ng/ml each of the indicated cytokines for 48 h. Supernatants were then tested for NO production (mean ± SEM, $n = 3$ with two replicates per experiment). Statistical differences compared with control (unstimulated) were determined using one-way ANOVA, followed by Bonferonni multiple comparison posttest (*$p < 0.05$, ***$p < 0.001$).

porters) are efficient in maintaining proper physiological concentrations of glutamate (60); however, perturbations in glutamate transporter expression can also contribute to excitotoxic cell death (61, 62). Cytokines are known to reduce glutamate transporter expression in astrocytes (63, 64), suggesting that during inflammatory conditions glutamate release through the system x_c^- transporter cannot be properly regulated by glutamate transporters. Pharmacologically inhibiting glutamate receptors or increasing glutamate transporter expression to confer protection is not likely feasible due to the imperative nature of glutamatergic signaling for normal physiological processes. This rationale makes identifying and blocking the source of excitotoxic glutamate a more practical therapeutic strategy.

As demonstrated in this manuscript, inflammation leads to excitotoxicity because cell death is blocked by the glutamate receptor antagonist NBQX. Release of glutamate from the system x_c^- transporter is a well-known source of glutamate toxicity during energy failure (16, 21, 42, 43). In exchange for the import of L-cystine, an important metabolite for glutathione, the system x_c^- transporter exports glutamate. Glutamate release from the

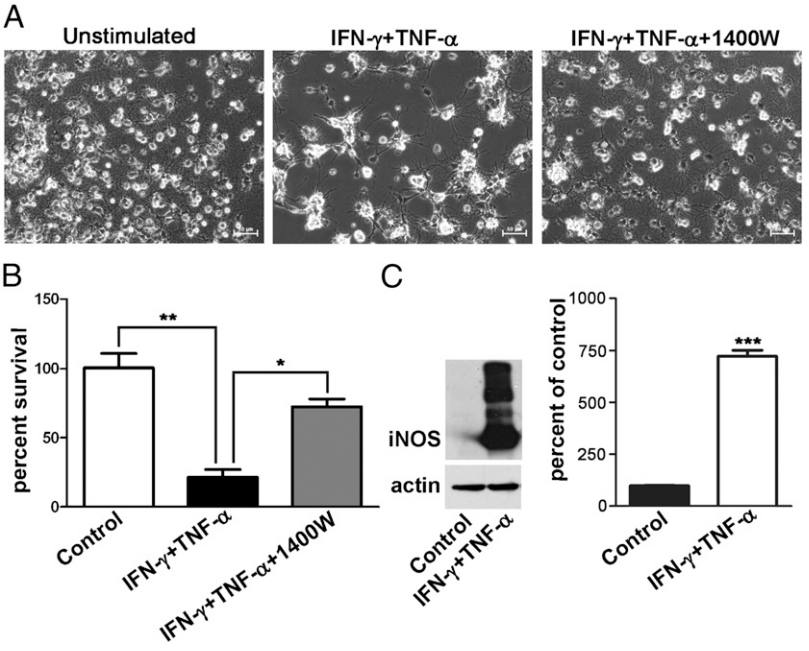

FIGURE 11. The iNOS inhibitor 1400W blocks mature OL death induced by cytokine-activated microglia. (**A**) Phase-contrast images of microglia (1×10^5) plated onto mature OLs and stimulated with IFN-γ and TNF-α in the presence or absence of 25 μM 1400W. Scale bars, 50 μm. (**B**) Differences in cell counts for IFN-γ and TNF-α in the presence or absence of 1400W are shown as percentage of control (unstimulated; mean ± SEM, $n = 3$ independent experiments with four replicates per experiment). Statistical differences determined using one-way ANOVA, followed by Bonferonni multiple comparison posttest (*$p < 0.05$, **$p < 0.01$). Similar results were obtained with 200 μM aminoguanidine hydrochloride, another iNOS inhibitor (data not shown). (**C**) Western blot (*left panel*) and densitometric analysis (*right panel*) of iNOS expression in microglia in the absence or presence of IFN-γ and TNF-α (mean ± SEM, $n = 3$). Statistical differences compared with control (unstimulated) were determined using a *t* test (***$p < 0.001$).

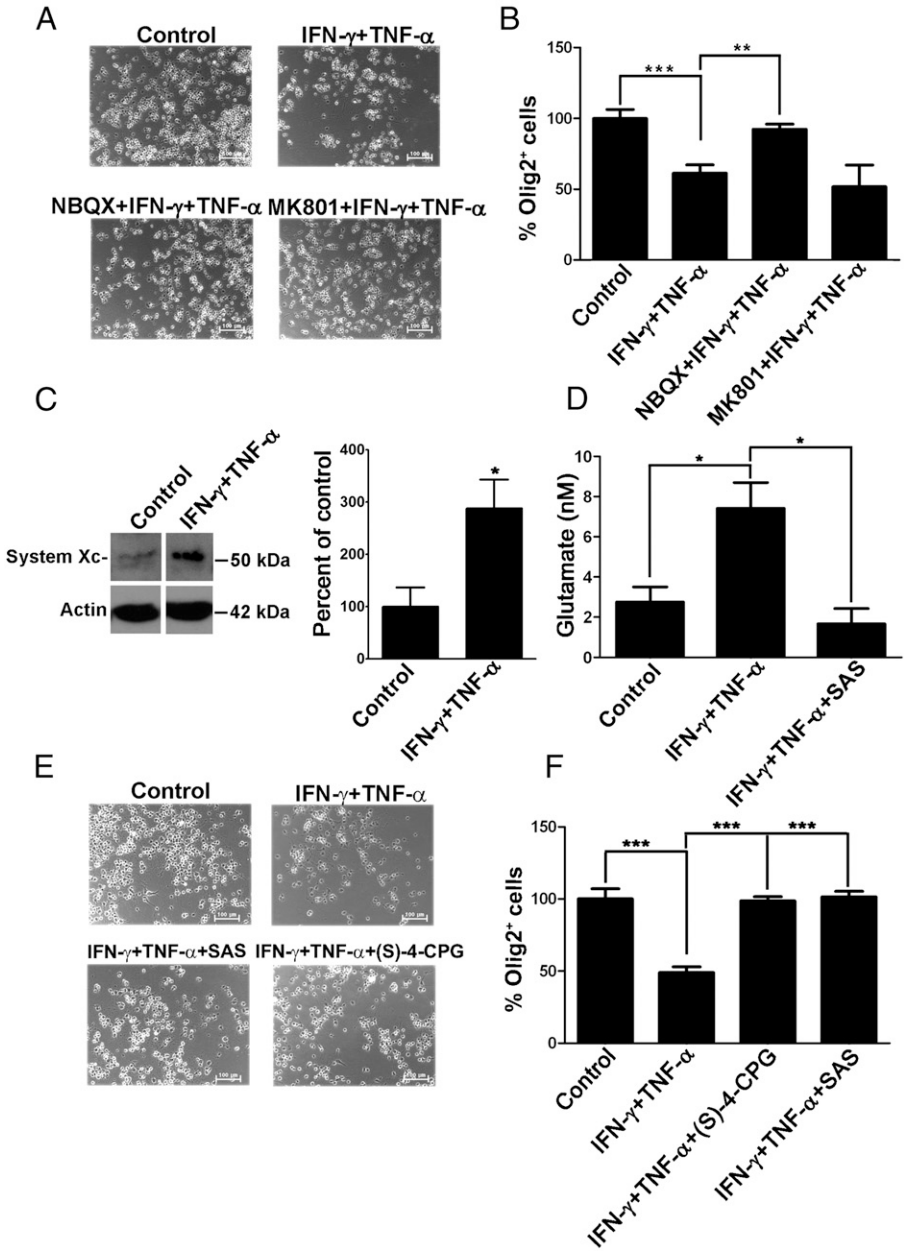

FIGURE 12. IFN-γ– and TNF-α–stimulated microglia induce AMPA receptor-dependent mature OL excitotoxicity by glutamate release through the system $_{Xc}^-$ transporter. (**A**) Purified microglia (1×10^5) were plated onto mature OLs and treated with NBQX (100 μM) or MK801 (10 μM) 1 h prior to treatment with IFN-γ and TNF-α (100 ng/ml each) for 12 h. Shown are representative phase-contrast images from three independent experiments. (**B**) Immunocytochemistry for Olig2 was performed to quantify the number of remaining mature OLs. Differences in cell counts for treatment with IFN-γ and TNF-α with or without NBQX or MK801 are expressed as percentage of control (mean ± SEM, $n = 3$ independent experiments with four replicates per experiment). (**C**) Western blot analysis of system $_{Xc}^-$ transporter expression in microglia exposed to IFN-γ (100 ng/ml), TNF-α (100 ng/ml), or in combination for 12 h. (**D**) Concentration of glutamate was measured in media from microglia treated for 12 h with IFN-γ and TNF-α (100 ng/ml each) in the presence or absence of SAS. Differences in ng glutamate are shown (mean ± SEM, $n = 3$ independent experiments with four replicates per experiment. (**E**) Purified microglia (1×10^5) were plated onto mature OLs and untreated or treated with IFN-γ and TNF-α (100 ng/ml each) for 12 h in the presence of the system $_{Xc}^-$ transporter antagonists SAS or S-4-CPG. Shown are representative phase-contrast images from three independent experiments. (**F**) Olig2 staining was performed to quantify the number of remaining OLs. Differences in cell counts for treatment with IFN-γ and TNF-α with or without SAS or S-4-CPG are expressed as percentage of control (mean ± SEM, $n = 3$ independent experiment with four replicates per experiment). Scale bars (A and E), 100 μm. (B, D, and F) Statistical differences were determined using one-way ANOVA, followed by Bonferonni multiple comparison posttest ($*p < 0.05$, $**p < 0.01$, $***p < 0.001$).

system $_{Xc}^-$ transporter has been demonstrated in cultured microglia after exposure to LPS and human peripheral monocytes from MS patients (30). Furthermore, in animal models of glioma, blocking glutamate release from the system $_{Xc}^-$ transporter prevented excitotoxicity to neurons (45, 65, 66). Consistent with these data, blocking the system $_{Xc}^-$ transporter ameliorated mature OL death from TNF-α/IFN-γ–stimulated microglia. In addition to blocking glutamate release from the system $_{Xc}^-$ transporter, SAS attenuates NF-κB, a key regulator of inflammation. Therefore, we tested S-4-CPG, another inhibitor of system $_{Xc}^-$ that does not have any effect on NF-κB (19), and demonstrated its effectiveness in alleviating OL excitotox-

icity in vitro. Although neonatally derived microglia is the most widely used approach, the activation profile of neonatally derived microglia in culture may not completely reflect what is observed in the adult rodent in vivo. These data warranted the exploration of this therapeutic target in animal models of MS.

Using the C57BL/6 animal model of EAE, treatment with system $_{Xc}^{-}$ transporter inhibitors SAS and S-4-CPG improved clinical scores. These data are consistent with myelin preservation in the spinal cord. It seems unlikely that the protective nature of SAS can be attributed to its role in inhibiting NF-κB because S-4-CPG, which has no mechanism of action at NF-κB, produced similar results. In culture, system $_{Xc}^{-}$ has been shown to affect T cell activation by redox modulation via macrophage and dendritic cells (67, 68). Therefore, i.p. injection of SAS was performed on day 7, after T cell activation has already occurred. This suggests that the lack of immune cell infiltration into the CNS in SAS-treated mice is an effect on T cell migration and not activation. Inhibitors of NF-κB do not have any effect on T cell infiltration into the CNS (69), supporting an important role for system $_{Xc}^{-}$ in T cell migration. Additionally, no reduction in T cell proliferation was found in spleens, suggesting that altering the function of system $_{Xc}^{-}$ did not affect T cell activation, but rather perturbed infiltration into the CNS. To further validate the role of the system $_{Xc}^{-}$ transporter in T cell migration, a nonpharmacological approach was undertaken. In this regard, we found that mice harboring a natural mutation in the gene encoding xCT were resistant to EAE compared with littermate controls. Similar to results from SAS-treated mice, T cell proliferation was not affected in system $_{Xc}^{-}$ deficient mice. Taken together, these data support a novel role for the system $_{Xc}^{-}$ transporter in regulating T cell infiltration into the CNS. Currently, two other studies have explored the effect of SAS in EAE induced in guinea pigs, but only report clinical assessments (70, 71).

The unexpected finding that SAS attenuates T cell infiltration into the CNS suggests that its protective nature may be due to attenuating T cell infiltration. To further explore the role of system $_{Xc}^{-}$ in CNS protection, we used a relapsing-remitting form of EAE and introduced SAS after the first relapse, therefore after T cell infiltration. SAS-treated animals showed improved clinical scores compared with PBS treated. Consistent with clinical outcomes, there was a reduction in reactive astrocytes, reactive microglia, and myelin damage in both the brain and spinal cord. These data support a novel role for the system $_{Xc}^{-}$ transporter in regulating pathogenesis after T cell infiltration in EAE.

Common therapies for MS block T cell infiltration into the CNS, which reduces, but does not eliminate, relapses. This warrants understanding the underlying mechanisms of how immune cells initiate CNS destruction to devise treatment strategies that also include CNS protection. We demonstrate that SAS is also protective to the CNS after T cell infiltration. This may have relevance to the clinical trial using SAS as a stand-alone therapy in MS. SAS treatment was beneficial during the first 18 mo, but at the 3-y time point no difference in Expanded Disability Status Scale score was observed compared with MS patients with no treatment (72). We propose that SAS may be more efficacious as an add-on therapy rather than a stand-alone treatment. Current therapies for MS do not protect the brain during symptomatic attacks, and using SAS as an add-on therapy may prove beneficial to quality of life and even disease progression.

The clinical data do support the efficacy of SAS as a treatment during the early acute phase of the inflammatory event because it was beneficial during the first 18 mo of treatment in MS. We show the efficacy of SAS in attenuating immune cell infiltration into the spinal cord during the initial inflammatory insult using the C57BL/6 chronic model of EAE. These data are consistent with preservation of spinal cord function and less damage to the myelin sheath. Transverse myelitis is an acute inflammatory demyelinating disease in which the immune system becomes primed to attack myelin in a specific segment of the spinal cord. Our data show that SAS blocks immune cell infiltration into the spinal cord in the acute onset of EAE, suggesting that SAS may be beneficial in an acute inflammatory demyelinating disease state such as transverse myelitis.

Acknowledgments

We thank the University of Alabama at Birmingham Comparative Pathology Laboratory, especially Trenton R. Schoeb for tissue preparation and histopathology services and Yan He and Sheila Shahidzadeh of Syracuse University for help with breeding and genotyping of the xCT-deficient mice. We also thank Dr. Harald Sontheimer from the University of Alabama at Birmingham for helpful discussions about system $_{Xc}^{-}$.

Disclosures

The authors have no financial conflicts of interest.

References

1. Pitt, D., E. Gonzales, A. H. Cross, and M. P. Goldberg. 2010. Dysmyelinated axons in shiverer mice are highly vulnerable to alpha-amino-3-hydroxy-5-methylisoxazole-4-propionic acid (AMPA) receptor-mediated toxicity. *Brain Res.* 1309: 146–154.
2. Lee, Y., B. M. Morrison, Y. Li, S. Lengacher, M. H. Farah, P. N. Hoffman, Y. Liu, A. Tsingalia, L. Jin, P. W. Zhang, et al. 2012. Oligodendroglia metabolically support axons and contribute to neurodegeneration. *Nature* 487: 443–448.
3. Follett, P. L., P. A. Rosenberg, J. J. Volpe, and F. E. Jensen. 2000. NBQX attenuates excitotoxic injury in developing white matter. *J. Neurosci.* 20: 9235–9241.
4. Manning, S. M., D. M. Talos, C. Zhou, D. B. Selip, H. K. Park, C. J. Park, J. J. Volpe, and F. E. Jensen. 2008. NMDA receptor blockade with memantine attenuates white matter injury in a rat model of periventricular leukomalacia. *J. Neurosci.* 28: 6670–6678.
5. DeSilva, T. M., and P. A. Rosenberg. 2012. Glutamate receptors, transporters, and periventricular leukomalacia. In *The Biology of Oligodendrocytes*. P. Armati and E. Mathey, eds. Cambridge University Press, New York, p. 186–201.
6. Wrathall, J. R., Y. D. Teng, and R. Marriott. 1997. Delayed antagonism of AMPA/kainate receptors reduces long-term functional deficits resulting from spinal cord trauma. *Exp. Neurol.* 145: 565–573.
7. Tekkök, S. B., and M. P. Goldberg. 2001. Ampa/kainate receptor activation mediates hypoxic oligodendrocyte death and axonal injury in cerebral white matter. *J. Neurosci.* 21: 4237–4248.
8. Matute, C., M. V. Sánchez-Gómez, L. Martínez-Millán, and R. Miledi. 1997. Glutamate receptor-mediated toxicity in optic nerve oligodendrocytes. *Proc. Natl. Acad. Sci. USA* 94: 8830–8835.
9. McDonald, J. W., S. P. Althomsons, K. L. Hyrc, D. W. Choi, and M. P. Goldberg. 1998. Oligodendrocytes from forebrain are highly vulnerable to AMPA/kainate receptor-mediated excitotoxicity. *Nat. Med.* 4: 291–297.
10. Pitt, D., P. Werner, and C. S. Raine. 2000. Glutamate excitotoxicity in a model of multiple sclerosis. *Nat. Med.* 6: 67–70.
11. Smith, T., A. Groom, B. Zhu, and L. Turski. 2000. Autoimmune encephalomyelitis ameliorated by AMPA antagonists. *Nat. Med.* 6: 62–66.
12. Groom, A. J., T. Smith, and L. Turski. 2003. Multiple sclerosis and glutamate. *Ann. N.Y. Acad. Sci.* 993: 229-275; discussion 287-288.
13. Bannerman, P., M. Horiuchi, D. Feldman, A. Hahn, A. Itoh, J. See, Z. P. Jia, T. Itoh, and D. Pleasure. 2007. GluR2-free alpha-amino-3-hydroxy-5-methyl-4-isoxazolepropionate receptors intensify demyelination in experimental autoimmune encephalomyelitis. *J. Neurochem.* 102: 1064–1070.
14. Stover, J. F., U. E. Pleines, M. C. Morganti-Kossmann, T. Kossmann, K. Lowitzsch, and O. S. Kempski. 1997. Neurotransmitters in cerebrospinal fluid reflect pathological activity. *Eur. J. Clin. Invest.* 27: 1038–1043.
15. Srinivasan, R., N. Sailasuta, R. Hurd, S. Nelson, and D. Pelletier. 2005. Evidence of elevated glutamate in multiple sclerosis using magnetic resonance spectroscopy at 3 T. *Brain* 128: 1016–1025.
16. Bridges, R. J., N. R. Natale, and S. A. Patel. 2012. System xc⁻ cystine/glutamate antiporter: an update on molecular pharmacology and roles within the CNS. *Br. J. Pharmacol.* 165: 20–34.
17. Lewerenz, J., S. J. Hewett, Y. Huang, M. Lambros, P. W. Gout, P. W. Kalivas, A. Massie, I. Smolders, A. Methner, M. Pergande, et al. 2013. The cystine/glutamate antiporter system x(c)(-) in health and disease: from molecular mechanisms to novel therapeutic opportunities. *Antioxid. Redox Signal.* 18: 522–555.
18. Nabeyama, A., A. Kurita, K. Asano, Y. Miyake, T. Yasuda, I. Miura, G. Nishitai, S. Arakawa, S. Shimizu, S. Wakana, et al. 2010. xCT deficiency accelerates chemically induced tumorigenesis. *Proc. Natl. Acad. Sci. USA* 107: 6436–6441.
19. Chung, W. J., and H. Sontheimer. 2009. Sulfasalazine inhibits the growth of primary brain tumors independent of nuclear factor-kappaB. *J. Neurochem.* 110: 182–193.
20. Domercq, M., M. V. Sánchez-Gómez, C. Sherwin, E. Etxebarria, R. Fern, and C. Matute. 2007. System xc- and glutamate transporter inhibition mediates microglial toxicity to oligodendrocytes. *J. Immunol.* 178: 6549–6556.

21. Jackman, N. A., S. E. Melchior, J. A. Hewett, and S. J. Hewett. 2012. Non-cell autonomous influence of the astrocyte system xc^- on hypoglycaemic neuronal cell death. *ASN Neuro* 4: e00074. Available at: http://asn.sagepub.com/content/4/1/AN20110030.full.
22. DeSilva, T. M., A. Y. Kabakov, P. E. Goldhoff, J. J. Volpe, and P. A. Rosenberg. 2009. Regulation of glutamate transport in developing rat oligodendrocytes. *J. Neurosci.* 29: 7898–7908.
23. Axtell, R. C., B. A. de Jong, K. Boniface, L. F. van der Voort, R. Bhat, P. De Sarno, R. Naves, M. Han, F. Zhong, J. G. Castellanos, et al. 2010. T helper type 1 and 17 cells determine efficacy of interferon-beta in multiple sclerosis and experimental encephalomyelitis. *Nat. Med.* 16: 406–412.
24. Sestero, C. M., D. J. McGuire, P. De Sarno, E. C. Brantley, G. Soldevila, R. C. Axtell, and C. Raman. 2012. CD5-dependent CK2 activation pathway regulates threshold for T cell anergy. *J. Immunol.* 189: 2918–2930.
25. Axtell, R. C., M. S. Webb, S. R. Barnum, and C. Raman. 2004. Cutting edge: critical role for CD5 in experimental autoimmune encephalomyelitis: inhibition of engagement reverses disease in mice. *J. Immunol.* 173: 2928–2932.
26. De Sarno, P., R. C. Axtell, C. Raman, K. A. Roth, D. R. Alessi, and R. S. Jope. 2008. Lithium prevents and ameliorates experimental autoimmune encephalomyelitis. *J. Immunol.* 181: 338–345.
27. Göbel, K., S. Bittner, T. Ruck, T. Budde, E. Wischmeyer, F. Döring, H. Wiendl, and S. G. Meuth. 2011. Active immunization with proteolipid protein (190-209) induces ascending paralysing experimental autoimmune encephalomyelitis in C3H/HeJ mice. *J. Immunol. Methods* 367: 27–32.
28. Muller, D. M., M. P. Pender, and J. M. Greer. 2000. A neuropathological analysis of experimental autoimmune encephalomyelitis with predominant brain stem and cerebellar involvement and differences between active and passive induction. *Acta Neuropathol.* 100: 174–182.
29. Albayram, O., J. Alferink, J. Pitsch, A. Piyanova, K. Neitzert, K. Poppensieker, D. Mauer, K. Michel, A. Legler, A. Becker, et al. 2011. Role of CB1 cannabinoid receptors on GABAergic neurons in brain aging. *Proc. Natl. Acad. Sci. USA* 108: 11256–11261.
30. Pampliega, O., M. Domercq, F. N. Soria, P. Villoslada, A. Rodríguez-Antigüedad, and C. Matute. 2011. Increased expression of cystine/glutamate antiporter in multiple sclerosis. *J. Neuroinflammation* 8: 63.
31. Wahl, C., S. Liptay, G. Adler, and R. M. Schmid. 1998. Sulfasalazine: a potent and specific inhibitor of nuclear factor kappa B. *J. Clin. Invest.* 101: 1163–1174.
32. Hepworth, M. R., L. A. Monticelli, T. C. Fung, C. G. Ziegler, S. Grunberg, R. Sinha, A. R. Mantegazza, H. L. Ma, A. Crawford, J. M. Angelosanto, et al. 2013. Innate lymphoid cells regulate CD4+ T-cell responses to intestinal commensal bacteria. *Nature* 498: 113–117.
33. Chintala, S., W. Li, M. L. Lamoreux, S. Ito, K. Wakamatsu, E. V. Sviderskaya, D. C. Bennett, Y. M. Park, W. A. Gahl, M. Huizing, et al. 2005. Slc7a11 gene controls production of pheomelanin pigment and proliferation of cultured cells. *Proc. Natl. Acad. Sci. USA* 102: 10964–10969.
34. Rasmussen, S., Y. Wang, P. Kivisäkk, R. T. Bronson, M. Meyer, J. Imitola, and S. J. Khoury. 2007. Persistent activation of microglia is associated with neuronal dysfunction of callosal projecting pathways and multiple sclerosis-like lesions in relapsing-remitting experimental autoimmune encephalomyelitis. *Brain* 130: 2816–2829.
35. Jäger, A., V. Dardalhon, R. A. Sobel, E. Bettelli, and V. K. Kuchroo. 2009. Th1, Th17, and Th9 effector cells induce experimental autoimmune encephalomyelitis with different pathological phenotypes. *J. Immunol.* 183: 7169–7177.
36. Kuchroo, V. K., and A. Awasthi. 2012. Emerging new roles of Th17 cells. *Eur. J. Immunol.* 42: 2211–2214.
37. Li, J., O. Baud, T. Vartanian, J. J. Volpe, and P. A. Rosenberg. 2005. Peroxynitrite generated by inducible nitric oxide synthase and NADPH oxidase mediates microglial toxicity to oligodendrocytes. *Proc. Natl. Acad. Sci. USA* 102: 9936–9941.
38. Axtell, R. C., C. Raman, and L. Steinman. 2013. Type I interferons: beneficial in Th1 and detrimental in Th17 autoimmunity. *Clin. Rev. Allergy Immunol.* 44: 114–120.
39. Sequeira, S. M., A. F. Ambrosio, J. O. Malva, A. P. Carvalho, and C. M. Carvalho. 1997. Modulation of glutamate release from rat hippocampal synaptosomes by nitric oxide. *Nitric Oxide* 1: 315-329.
40. Bal-Price, A., and G. C. Brown. 2001. Inflammatory neurodegeneration mediated by nitric oxide from activated glia-inhibiting neuronal respiration, causing glutamate release and excitotoxicity. *J. Neurosci.* 21: 6480–6491.
41. Brown, G. C. 2010. Nitric oxide and neuronal death. *Nitric Oxide* 23: 153-165.
42. Fogal, B., J. Li, D. Lobner, L. D. McCullough, and S. J. Hewett. 2007. System x(c)- activity and astrocytes are necessary for interleukin-1 beta-mediated hypoxic neuronal injury. *J. Neurosci.* 27: 10094–10105.
43. Jackman, N. A., T. F. Uliasz, J. A. Hewett, and S. J. Hewett. 2010. Regulation of system x(c)(-)activity and expression in astrocytes by interleukin-1β: implications for hypoxic neuronal injury. *Glia* 58: 1806–1815.
44. Bannai, S., and E. Kitamura. 1980. Transport interaction of L-cystine and L-glutamate in human diploid fibroblasts in culture. *J. Biol. Chem.* 255: 2372–2376.
45. Chung, W. J., S. A. Lyons, G. M. Nelson, H. Hamza, C. L. Gladson, G. Y. Gillespie, and H. Sontheimer. 2005. Inhibition of cystine uptake disrupts the growth of primary brain tumors. *J. Neurosci.* 25: 7101–7110.
46. Siffrin, V., H. Radbruch, R. Glumm, R. Niesner, M. Paterka, J. Herz, T. Leuenberger, S. M. Lehmann, S. Luenstedt, J. L. Rinnenthal, et al. 2010. In vivo imaging of partially reversible th17 cell-induced neuronal dysfunction in the course of encephalomyelitis. *Immunity* 33: 424–436.
47. Lee, S. C., D. W. Dickson, W. Liu, and C. F. Brosnan. 1993. Induction of nitric oxide synthase activity in human astrocytes by interleukin-1 beta and interferon-gamma. *J. Neuroimmunol.* 46: 19–24.
48. Chao, C. C., S. Hu, W. S. Sheng, D. Bu, M. I. Bukrinsky, and P. K. Peterson. 1996. Cytokine-stimulated astrocytes damage human neurons via a nitric oxide mechanism. *Glia* 16: 276–284.
49. Hewett, J. A., S. J. Hewett, S. Winkler, and S. E. Pfeiffer. 1999. Inducible nitric oxide synthase expression in cultures enriched for mature oligodendrocytes is due to microglia. *J. Neurosci. Res.* 56: 189–198.
50. Merrill, J. E., L. J. Ignarro, M. P. Sherman, J. Melinek, and T. E. Lane. 1993. Microglial cell cytotoxicity of oligodendrocytes is mediated through nitric oxide. *J. Immunol.* 151: 2132–2141.
51. Buntinx, M., E. Gielen, P. Van Hummelen, J. Raus, M. Ameloot, P. Steels, and P. Stinissen. 2004. Cytokine-induced cell death in human oligodendroglial cell lines. II: Alterations in gene expression induced by interferon-gamma and tumor necrosis factor-alpha. *J. Neurosci. Res.* 76: 846–861.
52. Buntinx, M., M. Moreels, F. Vandenabeele, I. Lambrichts, J. Raus, P. Steels, P. Stinissen, and M. Ameloot. 2004. Cytokine-induced cell death in human oligodendroglial cell lines: I. Synergistic effects of IFN-gamma and TNF-alpha on apoptosis. *J. Neurosci. Res.* 76: 834–845.
53. Hewett, S. J., J. A. Corbett, M. L. McDaniel, and D. W. Choi. 1993. Interferon-gamma and interleukin-1 beta induce nitric oxide formation from primary mouse astrocytes. *Neurosci. Lett.* 164: 229–232.
54. Vartanian, T., Y. Li, M. Zhao, and K. Stefansson. 1995. Interferon-gamma-induced oligodendrocyte cell death: implications for the pathogenesis of multiple sclerosis. *Mol. Med.* 1: 732–743.
55. Torres, C., I. Aránguez, and N. Rubio. 1995. Expression of interferon-gamma receptors on murine oligodendrocytes and its regulation by cytokines and mitogens. *Immunology* 86: 250–255.
56. Brenner, T., S. Brocke, F. Szafer, R. A. Sobel, J. F. Parkinson, D. H. Perez, and L. Steinman. 1997. Inhibition of nitric oxide synthase for treatment of experimental autoimmune encephalomyelitis. *J. Immunol.* 158: 2940–2946.
57. Brown, G. C., and A. Bal-Price. 2003. Inflammatory neurodegeneration mediated by nitric oxide, glutamate, and mitochondria. *Mol. Neurobiol.* 27: 325–355.
58. Mander, P., V. Borutaite, S. Moncada, and G. C. Brown. 2005. Nitric oxide from inflammatory-activated glia synergizes with hypoxia to induce neuronal death. *J. Neurosci. Res.* 79: 208–215.
59. Rousset, C. I., J. Kassem, P. Olivier, S. Chalon, P. Gressens, and E. Saliba. 2008. Antenatal bacterial endotoxin sensitizes the immature rat brain to postnatal excitotoxic injury. *J. Neuropathol. Exp. Neurol.* 67: 994–1000.
60. Tzingounis, A. V., and J. I. Wadiche. 2007. Glutamate transporters: confining runaway excitation by shaping synaptic transmission. *Nat. Rev. Neurosci.* 8: 935–947.
61. Tanaka, K., K. Watase, T. Manabe, K. Yamada, M. Watanabe, K. Takahashi, H. Iwama, T. Nishikawa, N. Ichihara, T. Kikuchi, et al. 1997. Epilepsy and exacerbation of brain injury in mice lacking the glutamate transporter GLT-1. *Science* 276: 1699–1702.
62. Sattler, R., and J. D. Rothstein. 2006. Regulation and dysregulation of glutamate transporters. *Handbook Exp. Pharmacol.* 175: 277–303.
63. Ye, Z. C., and H. Sontheimer. 1998. Glial glutamate transport as target for nitric oxide: consequences for neurotoxicity. *Prog. Brain Res.* 118: 241–251.
64. Ye, Z. C., and H. Sontheimer. 1996. Cytokine modulation of glial glutamate uptake: a possible involvement of nitric oxide. *Neuroreport* 7: 2181–2185.
65. Ye, Z. C., and H. Sontheimer. 1999. Glioma cells release excitotoxic concentrations of glutamate. *Cancer Res.* 59: 4383–4391.
66. Savaskan, N. E., A. Heckel, E. Hahnen, T. Engelhorn, A. Doerfler, O. Ganslandt, C. Nimsky, M. Buchfelder, and I. Y. Eyüpoglu. 2008. Small interfering RNA-mediated xCT silencing in gliomas inhibits neurodegeneration and alleviates brain edema. *Nat. Med.* 14: 629–632.
67. Gmünder, H., H. P. Eck, B. Benninghoff, S. Roth, and W. Dröge. 1990. Macrophages regulate intracellular glutathione levels of lymphocytes: evidence for an immunoregulatory role of cysteine. *Cell. Immunol.* 129: 32–46.
68. Yan, Z., S. K. Garg, J. Kipnis, and R. Banerjee. 2009. Extracellular redox modulation by regulatory T cells. *Nat. Chem. Biol.* 5: 721–723.
69. Brüstle, A., D. Brenner, C. B. Knobbe, P. A. Lang, C. Virtanen, B. M. Hershenfield, C. Reardon, S. M. Lacher, J. Ruland, P. S. Ohashi, and T. W. Mak. 2012. The NF-κB regulator MALT1 determines the encephalitogenic potential of Th17 cells. *J. Clin. Invest.* 122: 4698–4709.
70. Prosiegel, M., I. Neu, S. Vogl, G. Hoffmann, A. Wildfeuer, and G. Ruhenstroth-Bauer. 1990. Suppression of experimental autoimmune encephalomyelitis by sulfasalazine. *Acta Neurol. Scand.* 81: 237–238.
71. Prosiegel, M., I. Neu, G. Ruhenstroth-Bauer, G. Hoffmann, S. Vogl, L. Mehlber, and A. Wildfeuer. 1989. Suppression of experimental autoimmune encephalitis by sulfasalazine. *N. Engl. J. Med.* 321: 545–546.
72. Noseworthy, J. H., P. O'Brien, B. J. Erickson, D. Lee, D. Sneve, G. C. Ebers, G. P. Rice, A. Auty, W. J. Hader, A. Kirk, et al. 1998. The Mayo Clinic-Canadian Cooperative trial of sulfasalazine in active multiple sclerosis. *Neurology* 51: 1342–1352.